A NUMERICAL SIMULATION OF TWO-DIMENSIONAL SEPARATED FLOW IN A SYMMETRIC OPEN-CHANNEL EXPANSION USING THE DEPTH-INTEGRATED TWO-EQUATION (k-ε) TURBULENCE CLOSURE MODEL

by

Raymond Scott Chapman

Dissertation submitted to the Graduate Faculty of the
Virginia Polytechnic Institute and State University
in partial fulfillment of the requirements for the degree of
DOCTOR OF PHILOSOPHY
In
Civil Engineering

APPROVED:

C. Y. Kuo, Chairman

C. H. Lewis

H. W. Tieleman

B. H. Johnson

J. M. Wiggert

May, 1982

Blacksburg, Virginia

ACKNOWLEDGEMENTS

The author extends his sincerest thanks to the members of his advisory committee, Dr. Chin Y. Kuo, Dr. Clark H. Lewis, Dr. Henry W. Tieleman, Dr. James M. Wiggert, and (from the USAE Waterways Experiment Station, Vicksburg, Mississippi) Dr. Billy H. Johnson.

A significant portion of the present study was carried out while the author was on contract to the Environmental Laboratory of the USAE Waterways Experiment Station through an Intergovernmental Personnel Act Assignment Agreement with Virginia Polytechnic Institute and State University. Of the many people within WES that have provided valuable assistance, the author would particularly like to acknowledge the efforts of Mr. Ross W. Hall, Jr., Principal Investigator, Marsh Estuarine Modeling Team, and Mr. Donald L. Robey, Chief, Ecosystem Research and Simulation Division, Environmental Laboratory.

Finally, the author acknowledges the support of the National Science Foundation, grant No. CME-8004364, which made the initial phases of this study possible.

TABLE OF CONTENTS

CHAPTER 1

INTRODUCTION

In recent years, the field of computational hydraulics has matured at a remarkable rate of development. The reason for this rapid evolution is essentially two fold. Firstly, many of the problems encountered by hydraulic engineers, such as heat and mass transport, fluvial geomorphology, fluid structure interaction, and wave propagation, can not be adequately analyzed using close form linear or approximate solutions to the governing equations of motion. Secondly, the advent of larger and faster computers has made the use of sophisticated numerical techniques almost commonplace.

The role of the computer, and its impact on hydraulics in general, is uniquely characterized in the first paragraph of the preface of Computational Hydraulics (Abbott 1979) which reads:

> Very much as the steam engine was the principal physical instrument of the industrial revolution, so the digital computer is the principal physical instrument of our current "informational revolution". The digital computer's capacity to transform semantic information rapidly, reliably and cheaply, changes all technologies, even one with such long historical traditions as hydraulics. One of the first studies of the European enlightenment, investigated by da Vinci, Galileo, Newton and Euler, hydraulics had already been transformed through the industrial revolution into a 'productive benefit'. The current post-industrial revolution, concerned with directing investment into complex, finely balanced, 'high-information' machines and constructions, maintaining 'the highest information level per rate of information destruction', transform hydraulics again, adapting it to the new demands and the new possibilities of our modern societies.

One aspect of hydraulics that has been rather successful in adapting itself to modern technological needs is that area of computational

hydraulics that addresses the theory and computation of free surface flows. Much of this success is attributable to the fact that a wide range of engineering problems, which are complicated by free surface interaction, have been overcome by the introduction of the depth integrated equations of motion (Hansen 1962).

For this class of nearly horizontal free surface flow problems, the three-dimensional, time-averaged equations of fluid motion may be integrated over the vertical dimension thereby reducing the dynamical problem to solving for the horizontal depth-integrated velocities, and the water surface elevation. A consequence of spatially averaging the equations of motion is that additional closure approximations are required to represent the resulting bottom stress, wind stress, and the so called effective stresses. The effective stresses, as defined by Kuipers and Vreugdenhil (1973) consist of the depth-integrated viscous stresses, turbulent Reynold's stresses, and additional stresses which result from depth averaging the nonlinear convective acceleration terms (here after called momentum dispersion).

In an attempt to improve upon the current "state of the art" of free surface simulation models, the goal of the present study is to develop a two-dimensional depth-integrated hydrodynamic model capable of accurately predicting local regions of recirculation induced by abrupt changes in channel geometry. To accomplish this goal, it will be necessary to 1) implement a sufficiently accurate finite difference technique to minimize spurious numerical effects, and 2) employ a reasonable closure approximation for the effective stresses. The overall performance

of the simulation model will be assessed in a comparison of model predictions of steady, free surface, separated flow in a wide, shallow, rectangular channel with an abrupt expansion in width, with experimental measurements.

Literature Review

Experimental Measurement of Channel Expansion Flows

The first comprehensive study of separated, turbulent flow in a channel expansion was performed by Abbott and Kline (1962). Using a dye flow visualization technique Abbott and Kline examined the effects of the area ratio ($AR = 1 + W_1/W_o$) on the nondimensional reattachment length, x_r/W_1, for flow past single and double backward facing steps in a water channel (Figure 1). For area ratios greater than 1.5, Abbott and Kline showed that the expansion flow was asymmetric with the reattachment length on one side of the double step configuration being about three times that on the other. However, for area ratios less than 1.5, the reattachment lengths were symmetric and equal to a single step reattachment length ($x_r/W_1 = 7 \pm 1$) of the same area ratio.

Since the early work of Abbott and Kline (1962), a number of similar experimental studies of flow over backward facing steps have appeared in the literature. A review of these works may be found in Kim et al. (1978), Durst and Tropea (1981), and Eaton and Johnston (1981). An important point brought out by Durst and Tropea (1981), and Eaton and Johnston (1981) was that observed reattachment length varied considerably from one experimental investigation to the next. For

example, in a compilation of data for twelve independent experimental studies of symmetric channel expansion flow, Durst and Tropea (1981) show a variation in the observed nondimensional reattachment lengths of $4.5 \leq x_r/W_1 \leq 8$.

It has been suggested (Durst and Tropea 1981, Eaton and Johnston 1981) that much of the variation in the observed reattachment length is attributable to differences in 1) the area ratio, AR, of the expansion section and 2) the aspect ratio of the flow apparatus, h/W_1, where h is defined to be either the fluid depth, or the duct height. For symmetric channel expansion (AR < 1.5), Abbott and Kline (1962) showed the reattachment length to be reasonably constant, which suggests that the aspect ratio must be of greater importance for this class of expansion flows.

The effect of the aspect ratio of the channel was in fact studied by de Brederode and Bradshaw (1972) who discovered that the reattachment length was essentially unaffected if the aspect ratio was greater than about ten. However, they found that for a fully turbulent flow at the point of separation, the reattachment length decreased for aspect ratios less than ten.

The observation of de Brederode and Bradshaw may be further refined by simply plotting published measurements of reattachment lengths for symmetric channel expansions (single and double step) as a function of an aspect ratio, h/W_o, based on the inlet channel half-width, W_o, (Figure 2). The trend of decreasing reattachment length with decreasing aspect ratio is clearly illustrated in figure 3.

In addition to reattachment length measurements, detailed measurements of the velocity distribution within the recirculation region of symmetric expansions are presented by Etheridge and Kemp (1978), and Moss et al. (1977).

Effective Stress Concept

The first examination of the significance of the effective stresses was in a study on the generation of secondary flows presented by Kuipers and Vreugdenhil (1973). The basis of their theoretical analysis was the derivation of the depth-averaged vorticity equation. Conclusions drawn, that are of interest in the present work, were (1) vorticity is generated by the convergence and divergence of the depth mean velocity field, (2) the bottom stress acts to dissipate vorticity, and (3) the net moments of the effective stresses relative to vertical axis can generate vorticity in either direction.

It is interesting to note that in their secondary flow simulations, Kuipers and Vreugdenhil chose to neglect the effective stress terms; however, they do show that the effective stresses were represented in a fashion by the spatial smoothing procedure used to overcome nonlinear instability. Based on a comparison of predicted model results with hydraulic model studies, Kuipers and Vreugdenhil suggest: (1) secondary flow circulation can be predicted by a depth-integrated simulation model, (2) the convective acceleration terms must be retained, (3) horizontal eddies are not reproduced if less than five computational grid points cover its diameter, (4) the generation of eddies is sensitive

to the magnitude of the bottom friction coefficient, and (5) care must be taken in the treatment of wall boundaries.

The conclusions of Kuipers and Vreugdenhil have recently been verified in a paper by Ponce and Yabusaki (1981). In their study Ponce and Yabusaki adopted the work of Kuipers and Vreugdenhil and applied it to flow past a square cavity and a channel expansion.

Flokstra (1976, 1977) extended the theoretical work of Kuipers and Vreugdenhil (1973) by integrating the depth averaged vorticity equation, over a region of steady flow bounded by a closed streamline, to show that the dissipation of vorticity due to bottom friction is balanced exactly by the generation of vorticity by the effective shear stresses. As a result, he concluded that model simulations of main flow driven recirculation, performed with the effective stress neglected, show only the effects of numerical errors on the solution. By means of an energy balance, Flokstra further showed that momentum dispersion generally transfers energy out of the region of circulating flow leaving the turbulent Reynold's stresses to act as the mechanism which transforms energy into the region. Consequently, he concluded that with respect the effective stress closure, attention has to be concentrated mostly on modeling the effects of the depth-integrated Reynold's stresses.

Turbulent Reynold's Stress Closure

In the recent literature, the treatment of Reynolds stress closure has ranged from neglecting the terms to the concept of "large eddy" simulations (Leonard 1974) where, by means of spatial filtering of the equations of motions, only the small scale or "subgrid scale" Reynolds

stresses need be modeled. Within these two extremes lie a number of alternative closure schemes which exhibit a wide variation in complexity (Reynolds 1976).

One closure technique that has enjoyed considerable success in the simulation of a variety of turbulent flows is the two equation (k-ε) turbulence model described by Launder and Spalding (1974) and Rodi (1980). Applications of a depth-integrated version of the (k-ε) turbulence model have been presented by Rastogi and Rodi (1978), and McQuirk and Rodi (1978).

Rastogi and Rodi (1978) adopted the parabolized form of the depth-intergated equations of motion and (k-ε) turbulence model to simulate the problem of a coaxial jet issuing into a rectangular channel. By restricting their attention to a normal flow configuration with constant width, they were able to utilize the existing computational scheme of Patankar and Spalding (1972).

McQuirk and Rodi (1978) extended the use of the depth-averaged (k-ε) model to recirculating flows by simulating a side discharge, slot jet issuing normally into a rectangular channel. Forcing the free surface boundary to act as a "rigid lid" enabled them to apply the computation scheme of Gosman and Pun (1973), which was originally designed for the simulation of confined flows.

Although the results of the two model simulations appeared to compare well with experimental measurements, the general applicability of the models is limited by two significant problems. First, the specification of a "rigid lid" free surface boundary at best allows linear

variation in the water surface elevation which may not be adequate when modeling main flow driven recirculation. Secondly, the computational schemes adopted in both simulations are based on upwind differencing for the convective accelerations. Consequently, the simulation results could, in fact, have been tuned to experimental measurements, via numerical diffusion, by simply adjusting the nonuniform grid spacing (Castro 1977).

Momentum Dispersion Closure

The development of closure schemes for the momentum dispersion mechanism (Flokstra 1977, Abbott and Rasmussen 1977, Lean and Weare 1979) has, to date, solely been based on a simple helicoidal flow approximation, which allows the vertical variation of the horizontal velocity components to be modeled by known theoretical velocity distributions (Van Bendegom 1947, Rozovskii 1957, Engelund 1974). Although the theoretical velocity distributions used to obtain closure models for momentum dispersion were all derived under the assumption of fully developed flow in a long, channel bend, and subsequently do not strictly apply to flow through channel expansion; important information regarding the nature of the momentum dispersion mechanism can be gotten from these models. First, the net effect of the normal components of momentum dispersion is to increase the effective shear stress, irrespective of the degree of streamline curvature. Second, the magnitude of the transverse component of momentum dispersion, which can act to decrease the effective shear stress, is directly proportional to the ratio of the depth of flow to the radius of curvature of the depth-mean streamlines.

Nonetheless, any attempt at incorporating an illfounded closure

model for momentum dispersion, in the present study, would only serve to complicate the assessment of turbulence closure. Consequently, the direct representation of momentum dispersion mechanism will not be addressed herein, however, the indirect effect of momentum dispersion on turbulence closure will be discussed in Chapter 3.

Computational Method

Recently, higher order finite difference techniques have been successfully applied to strongly convective transport problems in both one and two dimensions (Abbott and Rassmussen 1977, Hinstup et al. 1977, Holly and Preissmam 1977, Leonard 1979, Leschziner 1980, Chapman and Kuo 1981, Leschziner and Rodi 1981, Han et al. 1981). One of the more notable techniques for steady flow problems is the QUICK (Quadratic Upstream Interpolation for Convective Kinematics) method developed by Leonard (1979). The QUICK finite difference technique, which is based on a conservation, control volume integral formulation possesses the desirable convective stability of upwind differencing, but is free of what is classically called numerical diffusion (Roache 1972).

Comparison of QUICK and upwind differencing shows QUICK to be far superior in turbulent transport simulations where practical grid spacing were used (Leonard et al. 1978, and Leschziner and Rodi 1981). It is interesting to note that both Leonard et al. 1978) and Leschziner and Rodi 1981), point out that when the standard (k-ε) turbulence model was modified to reflect the influence of streamline curvature (Bradshaw 1968, Launder et al. 1977, Militzer et al. 1977), the upwind difference solution exhibited no detectable response to closure modification, where as

a marked improvement was seen in the QUICK solution. The conclusion drawn in these studies was that the numerical diffusion introduced by upwind differencing simply overwhelmed the effects of streamline curvature modification.

Study Objective

The objective of the present study is to develop a two-dimensional, depth-integrated free surface hydrodynamic model capable of accurately simulating local regions of recirculation induced by abrupt changes in channel geometry. In order to accomplish this objective, the research program is divided into two phases:

(I) Development and testing of a depth-integrated hydrodynamic model, based on the QUICK finite difference technique, with effective stress closure neglected.

(II) A test application of the depth-integrated two-equation (k-ε) turbulence closure model for separated, free surface flow in a wide, shallow rectangular channel with an abrupt expansion in width.

The performance of the depth-integrated (k-ε) turbulence closure is evaluated by comparison of model simulations with published experimental data.

CHAPTER 2

DEPTH INTEGRATION OF THE EQUATIONS OF MOTION

Adopting tensor notation, the three dimensional, time-averaged equations of motion for an incompressible, homogeneous fluid with Coriolis forces neglected are written as follows:

Conservation of Mass

$$\frac{\partial v_i}{\partial x_i} = 0 \tag{1-1}$$

Conservation of Momentum

$$\frac{\partial v_i}{\partial t} + \frac{\partial (v_i v_j)}{\partial x_j} = -\frac{1}{\rho}\frac{\partial P}{\partial x_i} + g_i + \frac{\partial \sigma_{ij}}{\partial x_j} \tag{1-2}$$

where

v_i = time averaged velocity components (u, v, w)

x_i = Cartesian coordinate directions (x, y, z)

t = time

i,j = 1, 2, 3 and repeated indices require summation

ρ = fluid density

P = pressure

g_i = acceleration due to gravity (0, 0, -g)

σ_{ij} = shear stress tensor per unit mass

The shear stress tensor per unit mass σ_{ij} which includes both molecular and turbulent effects is written in the usual way:

$$\sigma_{ij} = -\overline{v_i' v_j'} + \nu \left(\frac{\partial v_i}{\partial x_j} + \frac{\partial v_j}{\partial x_i} \right) \qquad (1\text{-}3)$$

where

v_i' = turbulent velocity fluctuations

ν = kinematic viscosity

The right-handed orthogonal Cartesian coordinate system used in the present work is oriented such that the longitudinal direction, x, is positive to the right and the vertical direction, z, is positive upward. For puposes of illustration, a definition sketch is presented in figure 4.

Depth-Integration Process

For nearly horizontal flows with small depth to width ratios, it is appropriate to spatially average the equations of motion over the vertical dimension, z, thereby obtaining a depth-integrated representation of the flow field. As an example, consider the depth integration of the x-momentum equation presented by Kuipers and Vreugdenhil (1973). Defining z_b as the channel bottom elevation above some arbitrary datum, and h as the water depth, Leibnitz's rule is applied to

$$\int_{z_b}^{h+z_b} \left[\frac{\partial u}{\partial t} + \frac{\partial}{\partial x}(u^2) + \frac{\partial}{\partial y}(uv) + \frac{\partial}{\partial z}(uw) + \frac{1}{\rho}\frac{\partial P}{\partial x} - \frac{\partial}{\partial x}(\sigma_{xx}) - \frac{\partial}{\partial y}(\sigma_{xy}) \right] dz = 0$$

which when integrated becomes:

$$\frac{\partial}{\partial t}\int_{z_b}^{h+z_b} u\,dz + \frac{\partial}{\partial x}\int_{z_b}^{h+z_b} u^2\,dz + \frac{\partial}{\partial y}\int_{z_b}^{h+z_b} uv\,dz$$

$$\underset{(I)}{-\left[u_a\frac{\partial h}{\partial t} + u_a^2\frac{\partial}{\partial x}(h+z_b) + u_a v_a\frac{\partial}{\partial y}(h+z_b) - u_a w_a\right]}$$

$$\underset{(II)}{+\left(u_b^2\frac{\partial z_b}{\partial x} + u_b v_b\frac{\partial z_b}{\partial y} - u_b w_b\right)} + \frac{1}{\rho}\frac{\partial}{\partial x}\int_{z_b}^{h+z_b} P\,dz - \frac{P_a}{\rho}\frac{\partial(h+z_b)}{\partial x} \qquad (1\text{-}4)$$

$$+\frac{P_b}{\rho}\frac{\partial z_b}{\partial x} - \frac{\partial}{\partial x}\int_{z_b}^{h+z_b}\sigma_{xx}\,dz - \frac{\partial}{\partial y}\int_{z_b}^{h+z_b}\sigma_{xy}\,dz$$

$$\underset{(III)}{+\left[\sigma_{xxa}\frac{\partial}{\partial x}(h+z_b) + \sigma_{xya}\frac{\partial}{\partial y}(h+z_b) - \sigma_{xza}\right]}$$

$$\underset{(IV)}{-\left(\sigma_{xxb}\frac{\partial z_b}{\partial x} + \sigma_{xyb}\frac{\partial z_b}{\partial y} - \sigma_{xzb}\right)} = 0$$

where the subscripts a and b denote the free surface and channel bottom, respectively.

Recognizing that the terms labeled (I) and (II) correspond exactly to kinematic boundary conditions for the free surface and channel bottom, respectively, they must vanish. The term labeled (III) is the component of the wind shear stress tensor per unit mass acting along the free surface. The effect of wind forcing is not essential to the problem at hand and will subsequently be dropped from further discussion.

The term labeled (IV) is the component of the bottom shear stress tensor per unit mass acting in the plane of the channel bottom. With the assumption of a nearly horizontal free surface and channel bottom we can approximate term (IV) as a bulk bottom shear stress per unit mass, τ_{bx}. The parameterization of τ_{bx} will be discussed in Chapter 3.

The pressure terms in equation (1-4) can be handled in a consistent fashion by requiring that vertical accelerations are small compared to gravity. Hence the z-momentum equation reduces to:

$$\frac{\partial P}{\partial z} = -\rho g \tag{1-5}$$

Integrating and applying the boundary condition that the pressure equal atmosphere pressure at the free surface one obtains:

$$P = \rho g(h + z_b - z) + P_a$$

where P_a denotes atmospheric pressure. At this point, it will be assumed that atmospheric pressure is both uniform and equal to zero gage pressure. With the resulting hydrostatic approximation, the simplification of the remaining pressure terms

$$\frac{1}{\rho}\frac{\partial}{\partial x}\int_{z_b}^{h+z_b} P\, dz + \frac{P_b}{\rho}\frac{\partial z_b}{\partial x} \tag{1-6}$$

will proceed as follows:

$$\frac{1}{\rho}\frac{\partial}{\partial x}\int_{z_b}^{h+z_b} P\,dz = g\,\frac{\partial}{\partial x}\int_{z_b}^{h+z_b}(h + z_b - z)\,dz = g\,\frac{\partial}{\partial x}\left(\frac{h^2}{2}\right) \tag{1-7}$$

and similarly,

$$\frac{P_b}{\rho}\frac{\partial z_b}{\partial x} = gh\,\frac{\partial z_b}{\partial x} \tag{1-8}$$

Depth integration of the velocity components in the temporal and convective acceleration terms is accomplished by redefining the depth varying horizontal components, u and v, in terms of depth average values U and V and depth varying deviations, $\tilde{u}$ and $\tilde{v}$. The depth average values are defined by

$$U = \frac{1}{h}\int_{z_b}^{h+z_b} u\,dz \tag{1-9}$$

and

$$V = \frac{1}{h}\int_{z_b}^{h+z_b} v\,dz$$

such that

$$\int_{z_b}^{h+z_b} \tilde{u}\,dz = \int_{z_b}^{h+z_b} \tilde{v}\,dz = 0 \tag{1-10}$$

Following these rules the depth-averaged temporal and convective acceleration terms are rewritten:

$$\frac{\partial}{\partial t}\int_{z_b}^{h+z_b} u\,dz = \frac{\partial}{\partial t}(Uh) \tag{1-11}$$

$$\frac{\partial}{\partial x}\int_{z_b}^{h+z_b} u^2\,dz = \frac{\partial}{\partial x}(U^2h) + \frac{\partial}{\partial x}\int_{z_b}^{h+z_b} (u - U)^2\,dz \tag{1-12}$$

$$\frac{\partial}{\partial y}\int_{z_b}^{h+z_b} uv\,dz = \frac{\partial}{\partial y}(UVh) + \frac{\partial}{\partial y}\int_{z_b}^{h+z_b} (u - U)(v - V)\,dz \tag{1-13}$$

The second term on the right-hand side of equations (1-12) and (1-13) are momentum dispersion mechanisms which result from representing a non-uniform vertical boundary layer by a depth-averaged value of the velocity components.

Realizing the obvious symmetry in the depth integration process, the conservation of mass and y-momentum equations may be similarly integrated yielding the complete depth-integrated equations of motion, which when written in indicial form read:

Conservation of Mass

$$\frac{\partial h}{\partial t} + \frac{\partial (V_m h)}{\partial X_m} = 0 \tag{1-14}$$

Conservation of Momentum

$$\frac{\partial (V_m h)}{\partial t} + \frac{\partial (V_m V_n h)}{\partial X_n} + g\frac{\partial (h^2/2)}{\partial X_m} + gh\frac{\partial z_b}{\partial X_m} + \tau_{bm} - \frac{\partial T_{mn}}{\partial X_n} = 0 \tag{1-15}$$

in which

m,n = 1, 2 and repeated indices require summation;

V_m = two-dimensional depth-averaged velocity vector (U, V)

X_m = coordinate directions (x, y)

τ_{bm} = components of the bottom shear stress per unit mass

T_{mn} = components of the depth-integrated effective stress tensor per unit mass

The depth-integrated effective shear stress tensor as defined by Kuipers and Vreugdenhil (1973) and Flokstra (1977) contains the viscous stresses, the turbulent Reynold's stresses, and the momentum dispersion terms which arise from depth-integrating the nonlinear convective acceleration terms in the equations of motion. Specifically, the depth-integrated effective stress tensor per unit mass is written:

$$T_{mn} = \int_{z_b}^{h+z_b} \left[\nu \left(\frac{\partial v_m}{\partial X_n} + \frac{\partial v_n}{\partial X_m} \right) - \overline{v'_m v'_n} - (v_m - V_m)(v_n - V_n) \right] dz \qquad (1\text{-}16)$$

in which

v'_m = horizontal turbulent velocity fluctuations

The closure approximations adopted in the present work to represent the bottom shear stress, and effective stress mechanisms is the subject of the next chapter.

CHAPTER 3

CLOSURE MODELS

As in any turbulent flow simulation, a closure problem exists due to the presence of more unknowns than governing equations. The closure problem associated with the use of the depth-integrated equations of motion, in the present study, requires the parameterization of: (1) the bottom shear stress, (2) the depth-averaged turbulent Reynold's stresses, and (3) the momentum dispersion terms. In this chapter, the closure models adopted to represent these mechanisms will be discussed.

Bottom Shear Stress Closure

The bottom shear stress per unit mass is parameterized in accordance with the well-known quadratic shear stress law (Schlichting 1955), namely

$$\tau_b = cq^2 \tag{3-1}$$

where

τ_b = magnitude of the resultant bottom shear stress vector per unit mass (τ_{bx}, τ_{by})

c = drag coefficient for water flowing over a fixed surface

q = magnitude of the resultant velocity vector (U, V)

Defining theta (θ) to be the angle that lies between the resultant velocity vector and the x-axis, the vector components of the resultant shear stress per unit mass are written:

$$\tau_{bx} = cq^2 \cos \Theta$$

and

$$\tau_{by} = cq^2 \sin \Theta \tag{3-2}$$

Noting that

$$U = q \cos \Theta$$

and

$$V = q \sin \Theta \tag{3-3}$$

the familiar form of the bottom stress closure model is written

$$\tau_{bm} = cV_m q \tag{3-4}$$

where

$$q = (U^2 + V^2)^{1/2} \tag{3-5}$$

The value of the drag coefficient can be related to the channel roughness, z_o, and depth, h, by assuming that the vertical boundary layer in the central portion of an unidirectional, fully developed

turbulent open channel flow is adequately described by the logarithmic velocity law:

$$u(z) = \frac{U_*}{\kappa} \ell n \left(\frac{z}{z_o}\right) \tag{3-6}$$

where

U_* = shear velocity, $(\tau_{bx})^{1/2}$

κ = von Karman's constant

By definition,

$$U_*^2 = cU^2 \tag{3-7}$$

where again U is the depth-averaged velocity, and thus

$$c = \left[\frac{\kappa}{\ell n \left(\frac{\hat{z}}{z_o}\right)}\right]^2 \tag{3-8}$$

where $\hat{z}$ is the distance from the channel bottom where $u(\hat{z}) = U$. The value of $\hat{z}$ is obtained by first recalling that

$$U = \frac{1}{(h - z_o)} \int_{z_o}^{h} u(z)\, dz \tag{3-9}$$

or

$$U = \frac{U_*}{\kappa} \left[\left(\frac{h}{h - z_o}\right) \ell n \left(\frac{h}{z_o}\right) - 1\right] \tag{3-10}$$

Then combining equation (3-10) and equation (3-6) and simplifying yields

$$\hat{z} = z_o e^{-1} \left(\frac{h}{z_o}\right)^{\beta} \tag{3-11}$$

where

e = exponential function

$\beta = \dfrac{h}{h - z_o}$

Substitution of equation (3-11) into equation (3-8) yields an exact functional relationship for c in terms of channel roughness and depth, specifically:

$$c = \left[\frac{\kappa}{\beta \ell n \left(\frac{h}{z_o}\right) - 1}\right]^2 \tag{3-12}$$

It should be noted that equation (3-12) may be applied to flows without a fully developed boundary layer by simply replacing the depth, h, by an approximate boundary layer thickness.

Depth-Averaged Turbulent Reynold's Stress Closure

The turbulence closure model used herein is a modification of the depth-integrated $(k - \varepsilon)$ presented by Rastogi and Rodi (1978). The $(k - \varepsilon)$ turbulence model is based on the Boussinesq eddy viscosity hypothesis (Hinze 1975) which assumes that the turbulent Reynold's stresses

are proportional to the mean strain rates. Using three-dimensional tensor notation, the turbulent Reynold's stresses are written:

$$\overline{-v_i'v_j'} = -\frac{2}{3}k\delta_{ij} + \nu_t\left(\frac{\partial v_i}{\partial x_j} + \frac{\partial v_j}{\partial x_i}\right) \tag{3-13}$$

where

$k = \frac{1}{2}\overline{v_i'v_i'}$, the turbulent kinetic energy per unit mass

δ_{ij} = Kronecker delta

Unlike the molecular viscosity, ν , the turbulent eddy viscosity is flow dependent and can vary both in space and time. An approximation for the distribution of the turbulent eddy viscosity is obtained by assuming that it is proportional to the product of the characteristic velocity and length scale of turbulence, namely:

$$\nu_t \propto k^{1/2}\ell \tag{3-14}$$

where

ℓ = the macroscale of turbulence (a measure of the size of the energy containing eddies).

An inviscid estimate of the energy dissipation rate per unit mass, ε , is obtained when one assumes that the amount of energy dissipated at the small scales of turbulence equals the rate of supply at the large scales.

Again utilizing the characteristic velocity and length-scales of turbulence, dimensional considerations require that (Tennekes and Lumley 1972):

$$\varepsilon \sim \frac{k^{3/2}}{\ell} \tag{3-15}$$

Substitution of equation (3-15) into equation (3-14) yields a functional relationship for the turbulent eddy viscosity in terms of the kinetic energy of turbulence, k, and its rate of dissipation, ε, specifically:

$$\nu_t = C_\nu \frac{k^2}{\varepsilon} \tag{3-16}$$

where C_ν is an empirical coefficient.

In principal, solution of the exact transport equations for the turbulence kinetic energy, k, and its rate of dissipation, ε, enables one to completely specify the temporal and spatial distribution of the turbulent eddy viscosity. However, construction of the transport equations for k and ε result in additional closure problem. Consider first the turbulence kinetic energy equation (Hinze 1975):

$$\frac{\partial k}{\partial t} + \frac{\partial \left(k v_i\right)}{\partial x_i} = \frac{\partial}{\partial x_i}\left[\overline{v_i'\left(\frac{P'}{\rho} + k\right)}\right] - \left(\overline{v_i' v_j'}\right)\frac{\partial v_j}{\partial x_i} \qquad (3\text{-}17)$$

(I) (II)

$$+ \nu \frac{\partial}{\partial x_i}\left[\overline{v_j'\left(\frac{\partial v_i'}{\partial x_j} + \frac{\partial v_j'}{\partial x_i}\right)}\right] - \nu\overline{\left(\frac{\partial v_i'}{\partial x_j} + \frac{\partial v_j'}{\partial x_i}\right)\frac{\partial v_j'}{\partial x_i}}$$

(III) (IV)

where P' denotes turbulent pressure fluctuations, and the over-bar represents a time average. The closure problem results from the presence of the unknown pressure and velocity fluctuation correlations in term (I). Physically, term (I) represents the convective diffusion of the total turbulence mechanical energy per unit mass by turbulence. This term acts as a redistribution mechanism which suggests the use of a gradient diffusion model (Rodi 1980), or

$$\overline{v_i'\left(\frac{P'}{\rho} + k\right)} = \frac{\nu_t}{\sigma_k}\frac{\partial k}{\partial x_i} \qquad (3\text{-}18)$$

where σ_k is an empirical constant. Equation (3-13) may be substituted directly for the turbulent Reynold's stresses in the turbulence production term (II). Term (IV) is by definition the energy dissipation rate per unit mass, ε. Finally, term (III) represents the work done by the viscous shear stresses. For high Reynold's number flows, this term is small and can be neglected (Hanjalic and Launder 1972). Making the appropriate substitutions, the three-dimensional model equation for the turbulence kinetic energy is written:

$$\frac{\partial k}{\partial t} + \frac{\partial (v_i k)}{\partial x_i} = \frac{\partial}{\partial x_j}\left(\frac{\nu_t}{\sigma_k}\frac{\partial k}{\partial x_j}\right) + \nu_t\left(\frac{\partial v_i}{\partial x_j} + \frac{\partial v_j}{\partial x_i}\right)\frac{\partial v_i}{\partial x_j} - \varepsilon \qquad (3\text{-}19)$$

The exact transport equation for the energy dissipation rate per unit mass, for large Reynold's number, reads (Harlow and Nakayama 1968):

$$\frac{\partial \varepsilon}{\partial t} + \frac{\partial}{\partial x_i}(\varepsilon v_i) = -2\nu \frac{\partial v_i}{\partial x_r}\underbrace{\left(\overline{\frac{\partial v_i'}{\partial x_s}\frac{\partial v_r'}{\partial x_s} + \frac{\partial v_s'}{\partial x_i}\frac{\partial v_s'}{\partial x_r}}\right)}_{(I)}$$

$$-2\nu\underbrace{\left(\overline{\frac{\partial v_i'}{\partial x_r}\frac{\partial v_i'}{\partial x_s}\frac{\partial v_r'}{\partial x_s}}\right)}_{(II)} - 2\underbrace{\left(\overline{\nu\frac{\partial^2 v_i'}{\partial x_r \partial x_s}}\right)^2}_{(III)} \qquad (3\text{-}20)$$

$$-\underbrace{\frac{\partial}{\partial x_j}\overline{(v_j'\varepsilon')}}_{(IV)} - \underbrace{\frac{\nu}{\rho}\frac{\partial}{\partial x_i}\left(\overline{\frac{\partial p'}{\partial x_s}\frac{\partial v_i'}{\partial x_s}}\right)}_{(V)}$$

where

r,s = 1, 2, 3 and repeated indices require summation

ε' = turbulent fluctuations of the energy dissipation rate per unit mass.

The closure approximations for equation (3-20) were first presented by Hanjalic and Launder (1972). Their approach was to parameterize (I)-(III) in terms of the Reynold's stresses, mean strain rate, turbulence kinetic energy, and its rate of dissipation per unit mass, and neglect term (V) on the basis of being small. Term (I) represents the production mechanism for ε and was approximated accordingly,

$$(I) = -C_1 \left(\frac{\varepsilon}{k}\right) \overline{\left(v_i' v_r'\right)} \frac{\partial v_i}{\partial x_r} \tag{3-21}$$

Terms (II) and (III) were grouped together and parameterized as follows:

$$(II) + (III) = C_2 \frac{\varepsilon^2}{k} \tag{3-22}$$

The argument used to support equation (3-22) was that the sum of term (II), which represents the generation rate of vorticity fluctuations due to the self-stretching mechanism, and term (III), which represents the viscous decay of dissipation, should be controlled by the dynamics of the energy cascade. Subsequently, if the Reynold's number is sufficiently large to allow the existence of an inertial subrange an inviscid estimate based on dimensional considerations should be appropriate. Term (IV) represents the turbulent diffusion of ε which clearly suggests a closure of the form:

$$(IV) = \frac{\nu_t}{\sigma_\varepsilon} \frac{\partial \varepsilon}{\partial x_j} \tag{3-23}$$

where σ_ε is an empirical constant. Collecting the various approximations yields the complete model equation for the energy dissipation rate per unit mass:

$$\frac{\partial \varepsilon}{\partial t} + \frac{\partial (v_i \varepsilon)}{\partial x_i} = \frac{\partial}{\partial x_j}\left(\frac{\nu_t}{\sigma_\varepsilon} \frac{\partial \varepsilon}{\partial x_j}\right) + C_1 \nu_t \frac{\varepsilon}{k}\left(\frac{\partial v_i}{\partial x_j} + \frac{\partial v_j}{\partial x_i}\right) \frac{\partial v_i}{\partial x_j} - \frac{C_2 \varepsilon^2}{k} \tag{3-24}$$

Estimates for the empirical constants found in equations (3-19) and (3-24) were obtained by applying the model equations to simple turbulent flows for which experimental data were available. For example, in a local equilibrium, two-dimensional, boundary layer the production of turbulence energy is balanced by dissipation and Equation (3-19) reduces to:

$$\overline{u'v'} \frac{\partial u}{\partial y} = \varepsilon \tag{3-25}$$

A consistent closure approximation for the Reynold's stress is:

$$\overline{u'v'} = \nu_t \frac{\partial u}{\partial y} \tag{3-26}$$

which yields

$$\overline{u'v'}^2 = \nu_t \varepsilon \tag{3-27}$$

Now by definition,

$$\nu_t = C_\nu \frac{k^2}{\varepsilon} \tag{3-28}$$

thus, substitution of equation (3-27) into equation (3-26) results in

$$C_\nu^{1/2} = \frac{\overline{u'v'}}{k} \tag{3-29}$$

Experimental data (Ng and Spalding 1971) extracted from the work of Laufer (1954) suggests that $\overline{u'v'}/k$ varies from 0.22 to 0.3 which

gives a range of C_v from 0.05 to 0.09. The value of C_2 was found to to lie between 1.9 and 2.0 (Hanjalic and Launder 1972, and Launder et al. 1975) when computed using measured decay rates of the turbulent kinetic energy behind a grid (Batchelor and Townsend 1948, and Townsend 1956). The constant C_1 was obtained by examining the form of the dissipation equation in the constant shear stress region near the wall. Here convection is negligible with production and dissipation approximately in balance, thus

$$\varepsilon = \frac{U_*^3}{\kappa y} \tag{3-30}$$

Substituting equation (3-30) into equation (3-24) with some simplification yields

$$- \frac{\nu_t}{\sigma_\varepsilon} = (C_1 - C_2) \frac{U_*^3 y}{\kappa k} \tag{3-31}$$

In the near wall region (Townsend, 1956)

$$\nu_t = \kappa U_* y \tag{3-32}$$

thus

$$C_1 = C_2 - \frac{\kappa^2 k}{\sigma_\varepsilon U_*^2} \tag{3-33}$$

where by definition

$$\frac{U_*^2}{k} = C_V^{1/2} \tag{3-34}$$

and therefore

$$C_1 = C_2 - \frac{\kappa^2}{\sigma_\varepsilon C_V^{1/2}} \tag{3-35}$$

which specifies the value of C_1 when C_V, C_2, σ_k and σ_ε are known. The constants σ_k and σ_ε, which are similar to turbulent Prandtl or Schmidt Numbers, were assumed to be of order unity and determined along with the recommended values of the other constants via computer optimization. This was done by adjusting the values of the various constants until reasonable agreement between computed and experimental results were obtained. The values recommended by Launder and Spalding (1974) are as follows:

$$C_V = 0.09$$

$$C_1 = 1.44 \tag{3-36}$$

$$C_2 = 1.92$$

$$\sigma_k = 1.0$$

$$\sigma_\varepsilon = 1.3$$

With the appropriate specifications of boundary and initial conditions, equations (3-16), (3-19), (3-24), and (3-36) constitute the complete three-dimensional $(k - \varepsilon)$ turbulence closure model.

To be of use in approximating the depth-averaged Reynold's stress in equation (3-16) it is necessary to cast the three-dimensional $(k - \varepsilon)$ model into a depth-integrated form. Realizing that turbulence is inherently three dimensional, depth integration of the transport equations for the turbulence kinetic energy and its rate of dissipation cannot be strictly performed. However, Rastogi and Rodi (1978) suggest model equations for the depth-averaged turbulence energy, $\hat{k}$, and its rate of dissipation, $\hat{\varepsilon}$, can, in fact, be constructed if additional source terms are added to account for mechanisms originating from the nonuniformity of the flow over the vertical dimension. Furthermore, they suggest that the resulting turbulent viscosity, $\hat{\nu}_t$, should be interpreted such that when multiplied times the depth-averaged strain rate will yield the depth-averaged turbulent Reynold's stress. By analogy, the depth-averaged Reynold's stress tensor is written

$$\Sigma_{mn} = \hat{\nu}_t \left(\frac{\partial (V_m h)}{\partial X_n} + \frac{\partial (V_n h)}{\partial X_m} \right) - \frac{2}{3} \hat{k} h \delta_{mn} \tag{3-37}$$

where

$$\hat{\nu}_t = C_\nu \frac{\hat{k}^2}{\hat{\varepsilon}} \tag{3-38}$$

The resulting model equations for the depth-averaged value of the

turbulence energy, $\hat{k}$, and its rate of dissipation, $\hat{\varepsilon}$, are written as follows:

$$\frac{\partial(\hat{kh})}{\partial t} + \frac{\partial(V_m \hat{kh})}{\partial X_m} = \frac{\partial}{\partial X_m}\left[\hat{\nu}_t \frac{\partial(\hat{kh})}{\partial X_m}\right] + P_h + P_k - \hat{\varepsilon}h \qquad (3\text{-}39)$$

and

$$\frac{\partial(\hat{\varepsilon}h)}{\partial t} + \frac{\partial(V_m \hat{\varepsilon}h)}{\partial X_m} = \frac{\partial}{\partial X_m}\left[\frac{\hat{\nu}_t}{\sigma_\varepsilon} \frac{\partial(\hat{\varepsilon}h)}{\partial X_m}\right] + \frac{\hat{\varepsilon}}{\hat{k}}\left(C_1 P_h - C_2 \hat{\varepsilon}h\right) + P_\varepsilon \qquad (3\text{-}40)$$

where

$$P_h = \frac{\hat{\nu}_t}{h}\left[\frac{\partial(V_m h)}{\partial X_n} + \frac{\partial(V_n h)}{\partial X_m}\right]\frac{\partial(V_m h)}{\partial X_n} \qquad (3\text{-}41)$$

The source terms P_k and P_ε account for the production mechanism resulting from the presence of a vertical boundary layer. The form of these production terms may be obtained by considering the central portion of a unidirectional, uniform flow in a wide open channel. For this flow, the balance equations for $\hat{k}$ and $\hat{\varepsilon}$ reduce to

$$P_k = \hat{\varepsilon}h \qquad (3\text{-}42)$$

and

$$P_\varepsilon = C_2 \frac{\hat{\varepsilon}^2 h}{\hat{k}} \qquad (3\text{-}43)$$

To a good approximation, the total turbulence energy production over the vertical is written (Townsend 1956):

$$P_k = U_*^2 U \tag{3-44}$$

but by definition,

$$U_*^2 = cU^2 \tag{3-45}$$

therefore,

$$P_k = cU^3 \tag{3-46}$$

A similar relation may be obtained for the dissipation source P_ε by recalling that from equation (3-38)

$$\hat{k} = \left(\frac{\hat{\nu}_t \hat{\varepsilon}}{C_\nu}\right)^{1/2} \tag{3-47}$$

which may be substituted into equation (3-43) to yield

$$P_\varepsilon = \frac{C_2 C_\nu^{1/2} \hat{\varepsilon}^{3/2} h}{\hat{\nu}_t^{1/2}} \tag{3-48}$$

Noting that

$$\hat{\varepsilon} = \frac{U_*^2 U}{h} \tag{3-49}$$

and introducing the nondimensional dispersion coefficient

$$D = \frac{\hat{\nu}_t}{h U_*} \tag{3-50}$$

equation (3-48) is rewritten:

$$P_\varepsilon = \frac{C_2 C_v^{1/2} c^{5/4} U^4}{hD^{1/2}} \tag{3-51}$$

Generalizing these results to two dimensions is simply a matter of replacing the unidirectional flow velocity U with the magnitude of the resultant two-dimensional velocity vector q, specifically:

$$P_k = cq^3 \tag{3-52}$$

and

$$P_\varepsilon = \frac{C_2 C_v c^{5/4} q^4}{hD^{1/2}} \tag{3-53}$$

The interesting feature of this formulation is that introduction of the nondimensional dispersion coefficient in Equation 3-51 allows one to specify the value of the free stream turbulent eddy viscosity. Unfortunately, the value of D can vary over two orders of magnitude depending on the geometry of the channel, and in particular, how one interprets the mechanisms it represents. For example, if one interprets D as representing a vertical turbulent mixing coefficient, Elder (1959) shows that it assumes a value of about 0.07. Whereas, if one defines D to be a longitudinal dispersion coefficient for an infinitely wide open channel its value is approximately 5.9. Between these two extremes, an entire spectrum of values may be obtained if D is considered to be a transverse mixing coefficient. Depending on the cross-sectional

shape and the longitudinal curvature of the channel investigated, a compilation of numerous experiments yields values ranging from 0.1 to 1.0 (Fischer 1979). The actual specification of the nondimensional dispersion coefficient, D, in the present work, will be discussed in the next section.

Momentum Dispersion Closure

It was suggested in the introduction that existing closure schemes for the momentum dispersion mechanism lack sufficient theoretical and experimental justification to warrent direct consideration in the present work. However, the general effects of momentum dispersion can be indirectly investigated in the following way. First, the enhanced mixing due to vertical shear can be included in the (k-ε) turbulence closure model by appropriate specification of the nondimensional dispersion coefficient, D. In order to compare the effects of the specified momentum dispersion coefficient on the simulation results, a range of $0.2 \leq D \leq 5$ will be examined. Secondly, momentum transport due to curvature of the depth mean streamlines can be incorporated into the standard (k-ε) turbulence model by modifying the value of C_v in equation (3-38) when the streamline curvature is large. The approach used in the present study is an approximation to a method, based on an algebraic Reynold's stress model, presented by Leschziner and Rodi (1981). The necessity for including the streamline curvature modification, and its implementation is discussed in Chapter 6.

CHAPTER 4

COMPUTATIONAL METHOD

The numerical technique employed to obtain approximate solutions for the depth-integrated model equations is the third-order accurate QUICK (Quadratic Upstream Interpolation for Convective Kinematics) method developed by Leonard (1979). In this chapter, the derivation of QUICK which is based on a conservative, control volume integral formulation will be discussed. In addition, the inherent convective stability of the technique and the absence of classical numerical diffusion (Roache 1972) will be illustrated by comparison of QUICK with central and upwind differencing.

Control-Cell Formulation

To apply QUICK in a depth-integrated transport model, each equation must be integrated over its appropriate control cell on a constant space, staggered, square computation grid (Figure 5) and in time. For purposes of generality, it is first convenient to cast all of the model equations into the following vector form:

$$\frac{\partial Ft}{\partial t} + \frac{\partial Fx}{\partial x} + \frac{\partial Fy}{\partial y} = G \qquad (4\text{-}1)$$

where

$$Ft = \begin{Bmatrix} h \\ Uh \\ Vh \\ \hat{k}h \\ \hat{\varepsilon}h \end{Bmatrix} \quad ;$$

$$Fx = \begin{Bmatrix} Uh \\ UUh + \frac{gh^2}{2} - T_{xx} \\ UVh - T_{xy} \\ \hat{U}\hat{k}h - \nu_t \frac{\partial}{\partial x}(\hat{k}h) \\ U\hat{\varepsilon}h - \frac{\nu_t}{\sigma_\varepsilon}\frac{\partial}{\partial x}(\hat{\varepsilon}h) \end{Bmatrix} ;$$

$$Fy = \begin{Bmatrix} Vh \\ UVh - T_{xy} \\ VVh + \frac{gh^2}{2} - T_{yy} \\ \hat{V}\hat{k}h - \nu_t \frac{\partial}{\partial y}(\hat{k}h) \\ V\hat{\varepsilon}h - \frac{\nu_t}{\sigma_\varepsilon}\frac{\partial}{\partial y}(\hat{\varepsilon}h) \end{Bmatrix} ;$$

and

$$G = \begin{Bmatrix} 0 \\ gh\frac{\partial z_b}{\partial x} + \tau_{bx} \\ gh\frac{\partial z_b}{\partial y} + \tau_{by} \\ P_h + P_k - \hat{\varepsilon}h \\ \frac{\hat{\varepsilon}}{\hat{k}}(C_1 P_h - C_2 \hat{\varepsilon}h) + P_\varepsilon \end{Bmatrix} ;$$

in which all variables have been defined previously. The exact control cell integration of equation (4-1) may then be written:

$$\int_{-\frac{\Delta x}{2}}^{\frac{\Delta x}{2}} \int_{-\frac{\Delta y}{2}}^{\frac{\Delta y}{2}} \left(Ft^{n+1} - Ft^{n} \right) dx\, dy + \int_{0}^{\Delta t} \int_{-\frac{\Delta y}{2}}^{\frac{\Delta y}{2}} \left(Fx_R - Fx_L \right) dy\, dt$$

$$+ \int_{0}^{\Delta t} \int_{-\frac{\Delta x}{2}}^{\frac{\Delta x}{2}} \left(Fy_T - Fy_B \right) dx\, dt = \int_{0}^{\Delta t} \int_{-\frac{\Delta x}{2}}^{\frac{\Delta x}{2}} \int_{-\frac{\Delta y}{2}}^{\frac{\Delta y}{2}} G\, dy\, dx\, dt \qquad (4\text{-}2)$$

Noting that steady-state solution are sought, a simple Euler time integration is adopted which allows equation (4-2) to be rewritten as follows:

$$\underline{Ft}^{n+1} = \underline{Ft}^{n} - \frac{\Delta t}{\Delta s} \left[(Fx)_R - (Fx)_L + (Fy)_T - (Fy)_B \right]^{n} + \Delta t \underline{G}^{n} \qquad (4\text{-}3)$$

in which quantities in parentheses with subscripts R , L , T , and B denote right, left, top, and bottom cell face averages, respectively, and underlined quantities denote cell averages (Figure 6).

Derivation of QUICK

The cell and cell face averages that are required in equation (4-3) are approximated by integrating a six-point upstream weighted quadratic interpolation function over the appropriate limits. To illustrate this procedure, consider the computation the right cell face average of a field variable, f , using the information provided in figure 7. In this case, the U and V velocity components are both positive and directed to the right and up, respectively. Combining a Newton forward

difference interpolation formula in the longitudinal, ξ , direction with a Gauss backward difference interpolation formula in the transverse, η , direction, a quadratic interpolation function is constructed which reads (Hildebrand 1956):

$$f_{\xi,\eta} = (1 - \xi^2 - \eta^2 - \xi\eta)f_{0,0} + \left(\frac{\xi^2}{2} + \frac{\xi}{2} + \xi\eta\right)f_{1,0} + \frac{1}{2}(\xi^2 - \xi)f_{-1,0}$$

$$+ \frac{1}{2}(\eta^2 + \eta)f_{0,1} + \left(\frac{\eta^2}{2} - \frac{\eta}{2} + \xi\eta\right)f_{0,-1} - \xi\eta f_{1,-1} \qquad (4\text{-}4)$$

where $\xi = x/\Delta s$, and $\eta = y/\Delta s$ are local nondimensional coordinates. The right cell face average is then computed as follows:

$$(f)_R = \int_{-\frac{1}{2}}^{\frac{1}{2}} f_{1/2,\eta}\, d\eta = \frac{1}{2}(f_{0,0} + f_{1,0}) - \frac{1}{8}(f_{1,0} - 2f_{0,0} + f_{-1,0})$$

$$+ \frac{1}{24}(f_{0,1} - 2f_{0,0} + f_{0,-1}) \qquad (4\text{-}5)$$

Due to the symmetry of the integration operation, a change in the sign of the V velocity component will not alter equation (4-5). However, a change in the sign of the U velocity component will require that the mirror image of figure 7 be used with the indices shifted to the right by one. Performing the integration prescribed in equation (4-5) results in the following interpolation formula:

$$(f)_R = \frac{1}{2}(f_{0,0} + f_{1,0}) - \frac{1}{8}(f_{2,0} - 2f_{1,0} - f_{0,0}) + \frac{1}{24}(f_{1,1} - 2f_{1,0} + f_{1,-1}) \qquad (4\text{-}6)$$

The purpose of this adjustment is to maintain the upstream weighting of the interpolation formula. This all important feature of the technique is the subject of the next section.

Concept of Convective Sensitivity

By means of a simple analysis in one dimension, it is easily shown that the upstream weighting of the interpolation formula solely accounts for the impressive convective stability of QUICK. Following Leonard (1979), consider the pure convection of a scalar function ϕ moving positively from left to right through a control cell centered at the origin $(x = 0)$. Noting figure 8, the influx to the control cell is given by

$$\text{INFLUX} = -\frac{\partial U\phi}{\partial x} = \frac{U_L\phi_L - U_R\phi_R}{\Delta s} \qquad (4\text{-}7)$$

Defining the convective sensitivity (C.S.) of a finite difference approximation to be

$$\text{C.S.} = \frac{\partial}{\partial\phi_0}(\text{INFLUX}) \qquad (4\text{-}8)$$

it is clear that, for convective stability, the convective sensitivity must always be negative. In effect this is a boundedness condition

which requires the influx to the control cell to decrease as ϕ_o increases toward an asymtotic value, and visa versa. Without transverse variation, the convective sensitivity of QUICK is written:

$$\frac{C.S.}{QUICK} = \frac{1}{\Delta s}\frac{\partial}{\partial \phi_0}\left\{U_L\left[\frac{1}{2}(\phi_0 + \phi_{-1}) - \frac{1}{8}(\phi_0 - 2\phi_{-1} + \phi_{-2})\right]\right.$$

$$\left. - U_R\left[\frac{1}{2}(\phi_1 + \phi_0) - \frac{1}{8}(\phi_1 - 2\phi_0 + \phi_{-1})\right]\right\} \quad (4\text{-}9)$$

which upon simplification becomes:

$$\frac{C.S.}{QUICK} = \frac{3}{8}\left(\frac{U_L - 2U_R}{\Delta s}\right) \quad (4\text{-}10)$$

Thus, it is apparent that QUICK maintains convective stability given that:

$$2U_R > U_L \quad (4\text{-}11)$$

If the upstream weighted curvature term is omitted, thereby reducing the order of interpolation from quadratic to linear, the familiar central differencing formula results. The convective sensitivity for central differencing is written as follows:

$$\frac{C.S.}{CENTRAL} = \frac{1}{2}\left(\frac{U_L - U_R}{\Delta s}\right) \quad (4\text{-}12)$$

which implies that central differencing maintains convective stability when

$$U_R > U_L \tag{4-13}$$

For completeness, if a zero order interpolation is adopted (i.e. upwind differencing) the convective sensitivity becomes

$$\frac{C.S.}{Upwind} = -\frac{U_R}{\Delta s} \tag{4-14}$$

which suggests that upwind differencing always maintains convective stability.

Comparison of equations (4-11), (4-13), and (4-14) clearly illustrates the stabilizing effect of upstream weighting of the interpolation formula. At one extreme, it is seen that central differencing which does not upstream weight the interpolation has an intolerable convective stability restriction. Whereas at the other end of the spectrum, upwind differencing which is entirely upstream weighted is without a convective stability restriction.

Truncation Error Analysis

With respect to convective stability, upwind differencing has been shown to be far superior to both QUICK and central differencing. However, the general applicability of upwind differencing in practical computation is often obviated by the effects of first order truncation errors (i.e. numerical diffusion). In order to examine the formal truncation error of the QUICK approximation for the convection term, consider again the problem of pure convection but with the velocity assumed uniform and equal to one. The convective flux is then written

$$\frac{\partial \phi_0}{\partial x} = \frac{\phi_R - \phi_L}{\Delta s} \tag{4-15}$$

Substituting the appropriate QUICK formulas for ϕ_R and ϕ_L yields:

$$\frac{\partial \phi_0}{\partial x} \doteq \frac{1}{8\Delta s} (\phi_{-2} - 7\phi_{-1} + 3\phi_0 + 3\phi_1) \tag{4-16}$$

The truncation error for this approximation could be obtained by examining the remainder term after taking the difference of the two interpolation functions. However, an alternative approach is to obtain the truncation error by simply deriving the finite difference approximation by means of Taylor series exspansions. Writing ϕ_{-2}, ϕ_{-1}, and ϕ_1 as a Taylor series about ϕ_0 one obtains:

$$\phi_{-2} = \phi_0 - 2\Delta s\phi_0' + 2\Delta s^2\phi_0'' - \frac{4}{3}\Delta s^3\phi_0''' + \frac{2}{3}\Delta s^4\phi_0'''' + \text{h.o.t.} \tag{4-17}$$

$$\phi_{-1} = \phi_0 - \Delta s\phi_0' + \frac{\Delta s^2}{2}\phi_0'' - \frac{\Delta s^3}{6}\phi_0''' + \frac{\Delta s^4}{24}\phi_0'''' + \text{h.o.t.} \tag{4-18}$$

$$\phi_1 = \phi_0 + \Delta s\phi_0' + \frac{\Delta s^2}{2}\phi_0'' + \frac{\Delta s^3}{6}\phi_0''' + \frac{\Delta s^4}{24}\phi_0'''' + \text{h.o.t.} \tag{4-19}$$

Combining the appropriate scalar multiples of equations (4-17)-(4-19) and dropping all higher order terms results in:

$$3\phi_1 - 7\phi_{-1} + \phi_{-2} = -3\phi_0 + 8\Delta s\phi_0' + \frac{1}{2}\Delta s^4\phi_0'''' \qquad (4\text{-}20)$$

which upon rearrangement becomes:

$$\phi_0' = \frac{1}{8\Delta s}(\phi_{-2} - 7\phi_{-1} + 3\phi_0 + 3\phi_1) - \frac{1}{16}\Delta s^3\phi_0'''' \qquad (4\text{-}21)$$

The formal third order accuracy exhibited in equation (4-21) shows that QUICK is entirely free of what is classically called numerical diffusion.

Simplifying Assumption

Strict application of the two-dimensional QUICK method in obtaining approximations for the required cell and cell face averages in equation (4-1) is not a simple task. The appearance of products of field variable would necessitate the evaluation of integrals of products of interpolation function. With the occurrence of triple products in the convection terms, it is obvious that the amount of computational effort would be prohibitive. Consequently, it is necessary to assume that averages of products of field variables are reasonably well approximated by the products of the individual field variable average. For example, computation of the right cell face average for the square of a field variable would proceed as follows. First the field variable is decomposed into its cell face average $(f)_R$ and a variation along the cell face f_R^* where

$$\int_{-\frac{1}{2}}^{\frac{1}{2}} f_R^* \, d\eta = 0 \tag{4-22}$$

and thus

$$\int_{-\frac{1}{2}}^{\frac{1}{2}} f_R f_R \, d\eta = (f)_R^2 + \int_{-\frac{1}{2}}^{\frac{1}{2}} f_R^* f_R^* \, d\eta$$

Then, as a matter of convenience, the integral on the right-hand side is assumed small and neglected.

CHAPTER 5

MODEL SIMULATIONS

The test problems chosen for model simulation were steady, free surface flow in a wide, shallow, rectangular channel with and without an abrupt expansion in the width. A systematic program of numerical experimentation was performed in two phases. In the first phase, attention was focused on evaluation of the QUICK finite difference scheme as applied to the solution of the frictionally damped shallow water wave equations. Consequently, turbulence closure was neglected so that the convective stability of QUICK could be examined without the aid of the stabilizing effects of turbulent diffusion/dispersion. The second phase of computation consisted of essentially repeating the two test problems with the (k-ε) turbulence model incorporated in the hydrodynamic code. In this chapter, the details of the numerical experiments are presented.

Simulations Without Turbulence Closure

The model parameters chosen for the first phase of computation were a longitudinal channel slope of 0.005, a transverse channel slope of zero, a friction coefficient of 0.018, and an upstream normal depth of 4.73 ft which corresponds to an arbitrarily chosen flow rate per unit width of 30 $ft^3/sec/ft$.

Backwater Computation

For the channel simulation without an abrupt expansion, the flow

was required not to vary in the transverse direction which allowed a comparison of the computed water surface profile with a standard fourth-order Runge Kutta solution (Hildebrand 1956 and White 1974) of the well known gradually varied flow equation (Chow 1959).

The water surface elevation at the downstream boundary was arbitrarily fixed at a depth of 4.0 ft and the outflow velocity was computed using the mass conservation equation. Uniform flow was specified at the upstream boundary by requiring that the longitudinal gradients of the water surface elevation and the velocity equal zero. Using 100 grid points in the instream direction, of which half represented depth and half represented velocity locations, it was found that a grid spacing of 90.0 ft yielded a satisfactory approximation for uniform flow at the upstream boundary.

At the outset of the computation, all interior depth points were set equal to the upstream normal depth, and all velocity points were set to zero.

Channel Expansion Simulation

The abrupt channel expansion simulation was performed with an outlet to inlet channel width ratio of 1.5. In this computation, both velocity components and the normal gradient of the water surface elevation were specified to be zero at rigid walls. This was accomplished by defining image points outside of the computational domain such that interpolated values of cell averages or cell face averages of the velocity components, and the normal gradients of the water surface elevation that coincided with the wall boundary were exactly zero.

Subsequently, the position of the channel wall was chosen such that grid points for the transverse velocity component resided on the wall boundary (Figure 9), and grid points for the streamwise velocity component and water surface elevation were located one half of a grid spacing from the channel wall (Figure 10).

Symmetry was imposed at the channel center line by employing a reflection boundary condition. Here the normal gradients of the streamwise velocity component and the water surface elevation were set equal to zero. The treatment of the transverse velocity component is identical to that for a rigid wall boundary.

The upstream and downstream boundaries were positioned sufficiently far from the abrupt expansion so that the requirement of uniform flow (i.e., zero gradient) was met when a grid spacing of 90.0 ft was employed.

An essentially arbitrary initial condition was again used where all of the depths were set equal to the upstream normal depth, and all velocities were set to zero.

Simulations With Turbulence Closure

Wall Boundary Layer Computation

The first test problem performed using (k-ε) turbulence closure was the simulation of a fully developed turbulent wall boundary layer. This test simulation was chosen to examine the performance of the wall boundary formulation by comparison with available experimental data (Nakagawa et al. 1975).

The experimental setup of Nakagawa et al. was approximated by adopting a channel half width of 0.25 ft with the free surface and channel bottom assumed to be parallel and stress free. Consequently, the longitudinal gradients of the nontrivial field variables U, k, and ε, and the friction coefficient were set to zero. In other words, the test problem was effectively reduced to a one-dimensional simulation of flow between two parallel plates with boundary condition required only at the channel center line and wall.

A reflection boundary was employed at the channel center line by setting the normal gradient of U, k, and ε to zero. For convenience, the center-line boundary was located at the midpoint between the first two grid points.

The wall boundary was approximated by the "wall function" method of Launder and Spalding (1972). The beauty of wall function method is that the shear stress is matched at the wall boundary with the interior flow field, which obviates the need to resolve the near wall boundary layer. Thus, a much coarser grid may be used near the wall.

To apply the wall function method, it is necessary to assume that the near wall region is in local equilibrium so that the shear stress is constant and the logarithmic velocity law is valid. Thus, the shear velocity, U_*, may be related to the local velocity, U_w, defined at the nearest interior grid point, by

$$U_* = \frac{\kappa U_w}{\ln\left(\frac{\Delta y}{2z_o}\right)} \tag{5-1}$$

where again, the location of the wall boundary is defined between grid points. Recall that, by definition, the wall shear stress per unit mass is written:

$$\tau_w = U_*^2 \tag{5-2}$$

which suggests that the wall shear stress could, in fact, be obtained from equation (5-1). However, an interesting feature of the wall function method is the desire to build as much interior field information as possible into the wall shear stress equation. Consequently, equation (3-34) is used to recast equation (5-2) into the form:

$$\tau_w = C_V^{1/4} \, k_w^{1/2} \, U_* \tag{5-3}$$

which upon substitution of equation (5-1) yields:

$$\tau_w = \frac{\kappa C_V^{1/4} \, k_w^{1/2} \, U_w}{\ln \, (\Delta y / 2 z_o)} \tag{5-4}$$

A favorable attribute of equation (5-4) is that it preserves the sign of the wall shear stress vector.

Another interesting feature of the wall function method is that the near wall energy dissipation rate per unit mass, ε_w, is specified as a function of the local turbulence kinetic energy, k_w. The relationship used to fix ε_w is obtained by substituting equation (3-34) into a local form of equation (3-30), namely,

$$\varepsilon_w = \frac{C_\nu^{3/4} \, k_w^{3/2}}{\kappa(\Delta y/2)} \tag{5-5}$$

The near wall values of the velocity, U_w, and the turbulence kinetic energy per unit mass, k_w, are computed using their respective balance equations, but with the following modifications: (1) the normal gradient of U and k at the wall are set to zero, (2) the usual shear stress term is replaced by the computed wall shear stress, i.e.,

$$\nu_t \left.\frac{\partial U}{\partial y}\right|_{wall} = \tau_w \tag{5-6}$$

and (3) the dissipation term in the turbulence energy equation is modified to account for the large increase in dissipation rate in the near wall region, specifically:

$$\underline{\varepsilon} = \frac{1}{\Delta y - z_o} \int_{z_o}^{\Delta y} \varepsilon_w dy \tag{5-7}$$

which with some simplification becomes:

$$\underline{\varepsilon} = \frac{C_\nu^{3/4} k_w^{3/2} \ln (\Delta y/z_o)}{\kappa \Delta y} \tag{5-8}$$

The initial condition used in the wall boundary layer computation corresponded to a simple plug flow. Specifically, the initial velocity distribution across the channel was assumed uniform and equal to 0.5 ft/sec, with arbitrary, but nonzero, values specified for the turbulence quantities k and ε .

Channel Expansion Simulations

The final set of test simulations with (k-ε) turbulence closure were performed using a wide, rectangular open channel with an abrupt expansion in width. An area ratio of 1.45 was adopted for purposes of (1) insuring the validity of a centerline symmetry boundary, and (2) minimizing the number of superfluous grid points in the free stream.

The physical parameters specified for this series of computations were a longitudinal channel slope of 0.0005, a transverse channel slope of zero, and a friction coefficient of 0.0045 which corresponds to a roughness height, z_o , of 0.005. This combination of parameters results in a flow that is both fully turbulent and rough, which justifies the use of the quadratic shear stress law, and the logarithmic velocity law.

The nondimensional dispersion coefficient was specified at a nominal value of one for the initial set of test simulations, and subsequently, changed to 0.2 and 5 for purposes of examining its effect on the model results.

Wall boundaries were again approximated using the wall function technique; with a minor modification required to handle the convex corner of the abrupt exspansion. In the corner region, the top cell face of a U velocity cell, and the left cell face of a V velocity cell are divided equally between a wall and a fluid segment (Figure 11). Consequently, only one half of the predicted wall shear stress is used in the computation of these points.

The water surface elevation at the upstream boundary is specified to have zero gradient in the transverse direction, zero curvature in

the longitudinal direction, and a constant depth of 5.0 ft. This configuration corresponds to a unidirectional inflow boundary in which the transverse velocity component, V, is set to zero, and the longitudinal velocity component, U, is obtained from continuity. In addition, the turbulence quantities $\hat{k}h$ and $\hat{\varepsilon}h$ at the upstream boundary are assumed to have zero curvature in the longitudinal direction.

The downstream boundary configuration is essentially identical to the upstream boundary with the exception that the depth was set to 4.9 ft for purposes of accelerating convergence.

An initial condition for the (k-ε) turbulence closure simulations was generated by running a constant eddy viscosity version of the model to an approximate steady state. A steady state, constant eddy viscosity of 2.0 ft^2/sec was found to be consistent with the earlier assumption on the value of the nondimensional dispersion coefficient (i.e., $D = 1.0$). An arbitiary initial condition was used in the constant eddy viscosity computation with the interior water surface elevations set to 5.0 ft, and the velocity components set to zero.

CHAPTER 6

RESULTS AND DISCUSSION

In this chapter, the results of the model simulations described in Chapter 5 will be presented and discussed.

Results of Simulations Without Turbulence Closure

Backwater Computation

The simple straight wall channel simulation was performed using a stable time step of .75 sec. which resulted in an average one-dimensional Courant number [= $(q + \sqrt{gh})\ \Delta t/\Delta s$] of about .15. An arbitrarily chosen maximum difference, between the QUICK and Runge-Kutta solutions, of .01 percent was achieved in 540 iterations. Consequently, the comparison of the predicted water surface profiles provided in figure 12 shows extremely good agreement.

Expansion Channel Simulation

The second test simulation, which simply included an abrupt expansion in width, required 3500 iterations with a time step of .4 sec. to yield a steady solution. The convergence criteria used in this simulation was to require that the computed flowrates at the upstream and downstream boundaries differed by less than .01 percent. An average two-dimensional Courant number [= $(q + \sqrt{2gh})\ \Delta t/\Delta s$] was found to be about .1, and the CPU time required was approximately 12 min on an IBM 3032.

It is interesting to note that much of the required CPU time was

consumed "washing out" the rather arbitrary initial condition specified. As a result, a companion simulation was made using an initial water surface profile that decreased linearly in the vicinity of the expansion. In this run, the convergence criteria was satisfied in about 6 min. of CPU time.

The results of the abrupt expansion calculation are presented in figure 13, a vector plot of the depth-integrated resultant velocities, and figure 14, a three dimensional plot of the water surface elevations.

The significance of the results presented becomes readily apparent when one attempts to repeat the test computations using linear interpolation for the cell and cell face averages, i.e. central differencing. In trial calculations of the two test problems, central differencing failed to produce steady solutions in either case. The inability of the central difference procedure to achieve stable solutions results from the poor convective stability of the technique which leads to undamped error growth (Wiggles).

Stable solutions could have been obtained with the central differencing if sufficient eddy diffusion was introduced to satisfy the cell Reynolds number restriction (Roache 1972):

$$\frac{q\,\Delta s}{\hat{v}_t} < 2 \qquad (6\text{-}1)$$

However, the explicit introduction of "physical" diffusion in the central difference calculation, for purposes of satisfying the cell Reynolds number restriction, is essentially equivalent to using upwind

differencing, which implicitly introduces numerical diffusion with the steady state numerical diffusion coefficient given by:

$$\hat{\nu}_{num} = \frac{q\,\Delta s}{2} \tag{6-2}$$

The remarkable similarity seen in equations (6-1) and (6-2) is not a mere coincidence.

Convective stability gained at the expense of introducing explicit or implicit numerical diffusion is of little use if ones desire is to investigate turbulence closure models. Consequently, the use of QUICK in the present test application of the depth-integrated (k-ε) turbulence closure model is clearly supported.

Results of Simulations With Turbulence Closure

Wall Boundary Layer Simulation

The model predictions for the simple wall boundary layer simulation were obtained by repeating the computation with different pressure gradients (i.e. channel slopes) until a reasonable agreement between the predicted and experimental (Nakagawa et al. 1975) values of the free stream velocity, U_{max} and shear velocity, U_* was achieved (Table 1). A comparison of the model predictions with the experimental data of Nakagawa et al. (1975) are shown in figure 15, a nondimensional plot of the velocity defect profile, figure 16, the nondimensional distribution of the turbulence kinetic energy per unit mass, and figure 17, the

Table 1

Comparison of the Experimental and Predicted Values of the Free Stream Velocity, U_{max}, and the Shear Velocity, U_*

	Experiment (Nakagawa et al. 1975)	Model Prediction
Umax (ft/sec)	5.52×10^{-1}	6.19×10^{-1}
U_* (ft/sec)	2.66×10^{-2}	2.74×10^{-2}

nondimensional distubution of the energy dissipation rate per unit mass.

The close agreement between the model predictions and the experimental data is not surprising when one recalls that the empirical coefficients specified in the (k-ε) turbulence model were in fact originally "tuned" for constant pressure gradient wall boundary layers (Launder and Spalding 1974).

A final point worth discussion is the discrepency between the predicted turbulence energy per unit mass and the experimental data (Figure 16) near the channel centerline (y/h = 1.0). The apparent error results from the fact that the experimental measurements of Nakagawa et al. were actually of a vertical boundary layer in an open channel flow, and subsequently, reflect the presence of a free surface. Rodi (1981) argues that use of a symmetry boundary condition at the free surface does not account for the expected reduction in the length scale of turbulence. Consequently, the turbulence energy should in fact be over predicted in that region. Realizing that the free surface boundary problem is obviated in a depth integrated simulation model, no attempt was made at incorporating the recommended boundary correction (Rodi 1981) into the wall boundary computation.

Channel Expansion Simulation

The final set of simulations included (k-ε) turbulence closure in the channel expansion problem. In order to generate a region of recirculation in the constant eddy viscosity starting solution, it was necessary to adopt a grid spacing of 5.0 ft so that the value of the convective acceleration and turbulent transport terms were of the same order

of magnitude as the bottom friction terms. When grid spacings much larger than 5.0 ft were tested, recirculation was almost entirely inhibited.

Using a grid spacing of 5.0 ft in the simulation with (k-ε) turbulence closure, 4000 iterations with a stable time step of .01 sec were required to achieve a steady solution. The convergence criteria used in these simulations were that (1) the computed flowrates at the upstream and downstream boundaries differed by less than .1 percent, and (2) the distubutions of the turbulence quanties $\hat{k}h$ and $\hat{\varepsilon}h$, which were initialized at arbitrarily small, but nonzero, values were time invariant. With an average Courant number of about .05, each simulation required approximately 140 min of CPU time.

The results of the channel expansion calculation with (k-ε) closure are presented in figure 18, a contour sketch of the water surface elevations, figure 19, a vector plot of the depth-averaged resultant velocities, and figures 20, 21, and 22, a comparison of predicted longitudinal velocity profiles at three locations with the experimental measurements of Moss et al. (1977).

The aspect ratio (h/W_o) of the inlet channel was approximately .09 which suggests that one should expect a nondimensional reattachment length (x_r/W_1) in the range of 4.5 to 5.0 (Figure 3). However, it is seen in figure 19 that the predicted reattachment length is about 3.2, which corresponds to an error of 30 percent.

In order to compare the predicted velocity profiles with experimental measurements, it was first necessary to 1) rescale the

nondimensional x-axis such that the origin corresponded to the reattachment point, x_r/W_1, thereby removing the problem of variable reattachment lengths, and 2) normalize the predicted velocity distribution so that predicted and measured velocities in the free stream matched.

The agreement between the model predictions and experimental measurements within the region of recirculation (Figure 20) is satisfactory, however, the velocity profiles in the region bounding the reattachment point are noticably underpredicted (Figures 21 and 22).

The overall poor agreement between model predictions and experimental measurements is directly attributable to the overprediction of the depth-averaged eddy viscosity in the region of strong streamline curvature (Leschziner and Rodi 1981). In an attempt to improve the model predictions, an approximation to the streamline curvature modification of Leschziner and Rodi (1981) was employed. In their work, Leschziner and Rodi showed that the value of the coefficient C_V in equation (3-38) is significantly less than .09 in regions of strong streamline curvature. Consequently, as a first approximation, the value of C_V was decreased to .03 at all grid points interior to the wall function grid points in the region downstream of the step for a distance of $6W_1$. The value .03 was chosen on the basis that it represents a reasonable average over the distribution of C_V computed by Leschziner and Rodi (1981).

A comparison of the nondimensional depth-averaged eddy viscosity distributions computed with and without the ad hoc curvature modification is shown in figure 23. From a symptomatic point of view, the

curvature modification does, in fact, overcome the problem of overprediction of the depth averaged eddy viscosities, however, the degree of success can only be measured by the improvement upon the predictions for the reattachment length and the velocity profiles.

Examination of figure 24, a vector plot of the depth averaged velocities, reveals a significant increase in the nondimensional reattachment length x_r/W_1, resulting from curvature modification. The predicted value in this simulation is approximately $x_r/W_1 = 4.6$ which agrees well with the experimental measurement depicted in figure 3. In addition, a marked improvement is seen in the comparison of the velocity profiles in the region near reattachment (Figures 27 and 28).

The final set of test simulations were performed to investigate the effects of varying the nondimensional dispersion coefficient, D, on the model predictions. In addition to the previously described simulations with D equal to one, two more test computation, both of which included curvature correction, were run with D equal to 0.2 and 5.0, respectively.

For the case where the nondimensional dispersion coefficient was reduced to 0.2, the model responded with a 5 percent increase in the reattachment length, and a noticable, but slight increase in the velocity gradient across the recirculation zone (Figure 29). On the other hand, when D was increased to 5.0 the reattachment length decreased by 5 percent with a corresponding decrease in the velocity gradient across the recirculation region.

Insight into the proper specification of the nondimensional

dispersion coefficient, D, can be gained by examining figure 30, a comparison of the computed distributions of the depth-integrated eddy viscosity at the upstream boundary for varying values of D.

It is clear that when D is set to 0.2, the magnitude of the free stream eddy viscosity is underpredicted. This observation is easily argued on the basis that the near wall value of the eddy viscosity, which is fixed by the wall function, can not physically take on a value twice that of the free stream. Thus, a nondimensional dispersion coefficient of 0.2 appears to be too small.

Experimental measurements of flows in wide, rectangular channels (Rodi 1980) suggest that the wall boundary layer thickness is less than 20 percent of W_1, the channel half width. As a result, it seems reasonable that the depth-averaged eddy viscosity over 80 percent of the channel should be constant and solely dependent on bottom effects. Although this feature is represented well when D is equal to 0.2 and 1.0, respectively, the same can not be said when D is equal to 5.0. In this case, the depth averaged eddy viscosity varies significantly over 50 percent of the flow, which would suggest that the free stream value is overpredicted.

Consequently, the nominal value of one, originally chosen for the nondimensional dispersion coefficient, appears to be the most satisfactory.

CHAPTER 7

SUMMARY AND CONCLUSIONS

In summary, the objective of the present study has been to develop a two-dimensional depth-integrated free surface hydrodynamic model capable of accurately simulating local regions of recirculating flow induced by abrupt changes in channel geometry. This objective was successfully accomplished by attacking the problem in two phases.

The first phase focused on the development and testing of the depth-integrated hydrodynamic model without the effective stresses considered. The purpose of this phase was to examine the convective stability of QUICK under conditions where the smoothing effects of physical diffusion/dispersion were unimportant. Based on the numerical results presented, it is concluded that:

1. When applied to highly convective flow problems, QUICK is far superior to either central or upwind differencing in that it offers a high degree convective stability, but is free from classical numerical diffusion.

2. QUICK is ideally suited for use in basic research directed toward examining effective stress closure schemes.

The second phase of research concentrated on building adequate closure for the effective stresses into the hydrodynamic model. In this phase, attention was primarily focused on closure of the depth-integrated Reynolds stresses by means of the (k-ε) turbulence closure scheme. Although there was no direct attempt made at momentum dispersion

closure, the effects of momentum dispersion were examined indirectly, by investigating of the effects of streamline curvature, and the magnitude of the nondimensional dispersion coefficient on turbulence closure. Based on the test application of the (k-ε) turbulence closure model to the problem of separation in a wide, shallow rectangular channel with an aburpt expansion in width, the following conclusions are presented:

1. Use of the standard depth-integrated (k-ε) turbulence model resulted in an underprediction of 30 percent in the reattachment length, and a poor representation of velocity profile measurements near the reattachment point.

2. When an ad hoc curvature correction was applied in the (k-ε) scheme, a marked improvement in the model predictions resulted. Consequently, the effects of curvature of the depth mean streamlines has been shown significant, which suggests that future work is needed to differentiate between the contribution of momentum dispersion due to streamline curvature, and the need for curvature correction in the (k-ε) turbulence model.

3. Variation of the nondimensional dispersion coefficient, D, over a physically reasonable range of values resulted in noticeable changes in the predicted reattachment length and the depth-averaged velocity profiles. However, based on results presented herein, it must be concluded that a value of one is the most appropriate of those examined.

Model Limitations and Recommendations for Future Research

The fundumental problem which limits the general utility of the

present version of the model is its basic spatial and temporal structure.

The spatial structure of the code was designed using a constant space, square grid cell, which requires a uniform distribution of grid points over the computational domain. Consequently, flow simulations such as the channel expansion problem require an unusually large number of grid points to insure that the position of upstream, downstream, and free stream boundaries does not affect the solution in the region of interest.

In order to overcome this problem, the spatial structure of the code could be modified to (1) accept a simple variable grid spacing, or (2) transform the original governing equations by either an exponential stretch function or boundary-fitted coordinates. Any of the foremen-tioned alternatives would offer one the latitude to adjust the grid density where necessary, however, care must be taken to insure that the resulting quadratic interpolation functions are constructed and used properly.

The problem associated with the time step structure is that an explicit update procedure has been employed, which is bound by very restrictive temporal stability criteria. Consequently, the model is rather slow to converge to a steady state solution. Alternative methods for rectifying this problem are (1) retain the transient sense of the solution procedure and develop a semi-implicit or fully implicit tempo-ral update, or (2) drop the temporal terms and solve the resulting set of nonlinear matrix equations by the Newton-Raphson method.

Finally, it should be pointed out that the QUICK technique was

originally developed to solve steady state problems. If ones desire is to address transient phenomena then quadratic upstream interpolation must also be applied to the temporal terms, which results in the QUICKEST (Quadratic Upstream Interpolation for Convective Kinematics with Estimated Streaming Terms) method, which is third-order in both space and time. A complete description of QUICKEST is presented by its originator, Leonard (1979).

REFERENCES

Abbott, D. E., and S. J. Kline, "Theoretical and Experimental Investigation of Flow Over Single and Double Backward Facing Steps," Report MD-5, Thermosciences Division, Department of Mechanical Engineering, Stanford University, June 1961.

Abbott, D. E., and S. J. Kline, "Experimental Investigation of Subsonic Turbulent Flow Over Single and Double Backward Facing Steps," Journal of Basic Engineering, Transactions, ASME, Vol. 84, 1962.

Abbott, M. B., "A Pathology of Mathematical Modeling," Journal of Hydraulic Research, Vol. 14, No. 4, 1976.

Abbott, M. B., and C. H. Rasmussen, "On the Numerical Modeling of Rapid Expansions and Contractions in Models that are Two-Dimensional in Plan," Paper A104, 17th IAHR Congress, Baden-Baden, Germany, 1977.

Abbott, M. B., Computational Hydraulics: Elements of the Theory of Free Surface Flows, Pitman Publishing Limited, London, 1980.

Atkins, D. J., S. J. Maskell, and M. A. Patrick, "Numerical Predictions of Separated Flows," Numerical Methods in Engineering, Vol. 15, No. 1, 1980.

Bradshaw, P., and F. Y. F. Wong, "The Reattachment and Relaxation of a Turbulent Shear Layer," Journal of Fluid Mechanics, Vol. 52, No. 1, 1972.

Bradshaw, P., "Review of 'The Calculation of Turbulent Boundary Layers on Spinning and Curved Surfaces,' by B. E. Launder et al.," Journal of Fluids Engineering, Transactions, ASME, Vol. 99, No. 2, 1977.

Castro, I. P., "Numerical Difficulties in the Calculation of Complex Turbulent Flows," Proceedings, Symposium on Turbulent Shear Flow, Pennsylvania State University, Vol. 1, 1977.

Chapman, R. S. and C. Y. Kuo, "Application of a High Accuracy Finite Difference Technique to Steady Free Surface Flow Problems," Presented at the Joint ASME/ASCE Mechanics Conference, Boulder CO, June 1981.

Chow, V. T., Open Channel Hydraulics, McGraw-Hill Book Co., Inc., New York, 1959.

Davis, T. W., and D. J. Snell, "Turbulent Flow Over a Two-Dimensional Step and Its Dependence Upon Upstream Flow Conditions," Proceedings, Symposium on Turbulent Shear Flows, Pennsylvania State University, Vol. 1, 1977.

Durst, F., and A. K. Rastogi, "Theoretical and Experimental Investigations of Turbulent Flow With Separation," Proceedings, Symposium on Turbulent Shear Flows, Pennsylvania State University, Vol. 1, 1977.

Durst, F., and C. Tropea, "Turbulent, Backward-Facing Step Flows In Two-Dimensional Ducts and Channels," Proceedings, Third Symposium on Turbulent Shear Flows, University of California, Davis, Sept. 1981.

Eaton, J. K., and J. P. Johnston, "A Review of Research on Subsonic Turbulent Flow Reattachment," AIAA Journal, Vol. 19, No. 9, 1981.

Elder, J. W., "The Dispersion of Marked Fluid in Turbulent Shear Flow," Journal of Fluid Mechanics, Vol. 5, No. 4, 1959.

Engelund, F., Flow and Bed Topography in Channel Bends, Journal of the Hydraulics Division, ASCE, Vol. 100, No. HY11, 1974.

Etheridge, D. W., and P. H. Kemp, "Measurements of Turbulent Flow Downstream of a Rearward-Facing Step," Journal of Fluid Mechanics, Vol. 86, No. 3, 1978.

Fischer, H. B., E. J. List, R. C. Y. Koh, J. Imberger, and N. H. Brooks, Mixing in Inland and Coastal Waters, Academic Press, Inc., New York, 1979.

Flokstra, C., "Generation of Two-Dimensional Horizontal Secondary Currents," Delft Hydraulics Laboratory, Report S 163-II, 1976.

Flokstra, C., "The Closure Problem for Depth Averaged Two-Dimensional Flows," Paper A106, 17th LAHR Congress, Baden-Baden, Germany, 1977.

Garde, R. J., K. G. Ranga Raju, and R. C. Mirshra, "Subcritical Flow in Open Channel Exspansions," Irrigation and Power, Vol. 36, No. 1, 1979.

Gosman, A. D., W. M. Pun, A. K. Runchal, D. B. Spalding, and M. Wolfshtein, Heat and Mass Transfer in Recirculating Flows, Academic Press, London, 1969.

Han, T., J. A. C. Humphrey, and B. E. Launder, "A Comparison of Hybrid and Quadratic-Upstream Differencing in High Reynolds Number Elliptic Flows," Computer Methods in Applied Mechanics and Engineering, Vol. 29, 1981.

Hanjalic, K., and B. E. Launder, "Turbulence in Thin Shear Flows," Journal of Fluid Mechanics, Vol. 52, No. 4, 1972.

Harlow, F. H., and P. I. Nakayama, "Transport of Turbulence Energy Decay Rate," Los Alamos Scientific Laboratory Report LA-3854, University of California, 1968.

Harlow, F. H., and C. W. Hirt, "Generalized Transport Theory of Anisotropic Turbulence," Los Alamos Scientific Laboratory Report LA 4086, University of California, 1969.

Hildebrand, F. B., Introduction to Numerical Analysis, McGraw-Hill Book Co., Inc., New York, 1956.

Hinstrup, P., A. Kej, and U. Kroszynski, "A High Accuracy Two-Dimensional Transport-Dispersion Model for Environmental Applications," Paper B17, 17th IAHR Congress, Baden-Baden, Germany, 1977.

Hinze, J. O., Turbulence, McGraw-Hill Book Co., Inc., New York, 1959.

Hirsh, R. S., "Higher Order Accurate Difference Solutions of Fluid Mechanics Problems by Compact Difference Techniques," Journal of Computational Physics, Vol. 19, No. 1, 1975.

Irwin, H. P. A. H., and P. Arnot Smith, "Prediction of the Effects of Streamline Curvature on Turbulence," The Physics of Fluids, Vol. 18, No. 6, 1975.

Holly, F. M., and A. Preissman, "Accurate Calculations of Transport in Two Dimensions," Journal of the Hydraulic Division, ASCE, Vol. 103, No. HY11, 1977.

Kim, J., S. J. Kline, and J. P. Johnston, "Investigation of Separation and Reattachment of a Turbulent Shear Layer: Flow Over a Backward-Facing Step," Report MD-37, Thermosciences Division, Department of Mechanical Engineering, Stanford University, April 1978.

Kuipers, J., and C. B. Vreugdenhil, "Calculation of Two-Dimensional Horizontal Flow," Report S 163-1, Delft Hydraulics Laboratory, 1973.

Laufer, J., "Investigation of Turbulent Flow in a Two-Dimensional Channel," Report 1053, NACA, 1951.

Launder, B. E., and D. B. Spalding, Lectures in Mathematical Models of Turbulence, Academic Press, Inc., New York, 1972.

Launder, B. E., and D. B. Spalding, "The Numerical Calculation of Turbulent Flows," Computer Methods in Applied Mechanics and Engineering, Vol. 3, 1974.

Launder, B. E., C. H. Pridden, and B. I. Sharma, "The Calculation of Turbulent Boundary Layers on Spinning and Curved Surfaces," Journal of Fluids Engineering, Transactions, ASME, Vol. 99, No. 1, 1977.

Lau, Y. L., and B. G. Krishnappan, "Ice Cover Effects on Stream Flows and Mixing," Journal of the Hydraulics Division, ASCE, Vol. 107, No. HY10, 1981.

Lean, G. H., and T. J. Weare, "Modeling Two-Dimensional Circulating Flows," Journal of the Hydraulic Division, ASCE, Vol. 105, No. HY1, 1979.

Leenderste, J. J., "Aspects of a Computational Model for Long-Period Water Wave Propagation," RM-5297-DR, The Rand Corporation, Santa Monica, CA, May 1967.

Leonard, A., "Energy Cascade in Large-Eddy Simulations of Turbulent Fluid Flow," Advances in Geophysics, 18A, 1974.

Leonard, B. P., M. A. Leschziner, and J. McGuirk, "Third-Order Finite-Difference Method for Steady Two-Dimensional Convection," Proceedings of the International Conference on Numerical Methods in Laminar and Turbulent Flow, Swansea, July 1978.

Leonard, B. P., "A Stable and Accurate Convective Modelling Procedure Based on Quadratic Upstream Interpolation," Computer Methods in Applied Mechanics and Engineering, Vol. 19, 1979.

Leschziner, M. A., and W. Rodi, "Calculation of Strongly Curved Open Channel Flow," Journal of the Hydraulic Division, ASCE, Vol. 105, No. HY10, 1979.

Leschziner, M. A., "Practical Evaluation of Three Finite Difference Schemes For the Computation of Steady-State Recirculating Flows," Computer Methods in Applied Mechanics and Engineering, Vol. 23, 1980.

Leschziner, M. A., and W. Rodi, "Calculation of Annular and Twin Parallel Jets Using Various Discretization Schemes and Turbulence-Model Variations," Journal of Fluids Engineering, Transactions, ASME, Vol. 103, 1981.

McGuirk, J. J., and W. Rodi, "A Depth-Averaged Mathematical Model for the Near Field of Side Discharges into Open Channel Flow," Journal of Fluid Mechanics, Vol. 86, No. 4, 1978.

Mehta, P. R., "Flow Characteristics in Two-Dimensional Expansion," Journal of the Hydraulic Division, ASCE, Vol. 105, No. HY5, 1979.

Mellor, G., "Review of 'The Calculation of Turbulent Boundary Layers on Spinning and Curved Surfaces,' by B. E. Launder et al.," Journal of Fluids Engineering, Transactions, ASME, Vol. 99, No. 2, 1977.

Militzer, J., W. B. Nicoll, and J. A. Alpay, "Some Observations on the Numerical Calculation of the Recirculation Region of Twin Parallel Symmetric Jet Flow," Proceedings, Symposium on Turbulent Shear Flows, Pennsylvania State University, Vol. 1, 1977.

Moss, W. D., Baker, S., and L. J. S. Bradbury, "Measurements of Mean Velocity and Reynolds Stresses in Some Regions of Recirculating Flow," Proceedings, Symposium on Turbulent Shear Flows, Pennsylvania State University, Vol. 1, 1977.

Nakagawa, H., I. Nezu, and H. Ueda, "Turbulence of Open Channel Flow Over Smooth and Rough Beds," Proceedings, Japan Society of Civil Engineers, No. 241, 1975.

Patankar, S. V., and D. B. Spalding, Heat and Mass Transfer in Boundary Layers," Intertext Publishers, London, England, 1970.

Ponce, V. M., and S. B. Yabusaki, "Modeling Circulation in Depth-Averaged Flow," Journal of the Hydraulics Division, ASCE, Vol. 107, No. HY11, 1981.

Rastogi, A., and W. Rodi, "Prediction of Heat and Mass Transfer in Open Channels," Journal of the Hydraulic Division, ASCE, Vol. HY3, 1978.

Reynolds, W. C., "Computation of Turbulent Flows," Annual Review of Fluid Mechanics, Vol. 8, 1976.

Roache, P. J., Computational Fluid Dynamics, Hermosa Publishers, Albuquerque, NM, 1972.

Rodi, W., Turbulence Models and Their Application in Hydraulics: A State of the Art Review, Presented by the IAHR-Section on Fundamentals of Division II Experimental and Mathematical Fluid Dynamics, Delft, 1980.

Rozovskii, I. L., Flow of Water in Bends of Open Channels, Academy of the Sciences of the Ukranian SSR, Kieu, USSR (translation no. OTS 60-51133), Office of Technical Services, Washington, D.C., 1957.

Schamber, D. R., and B. E. Larock, "Numerical Analysis of Flow in Sedimentation Basins," Journal of the Hydraulics Division, ASCE, Vol. 107, No. HY5, 1981.

Schlichting, H., Boundary Layer Theory, McGraw-Hill Book Co., Inc., New York, 1955.

Smyth, R., "Turbulent Flow Over a Plane Symmetric Sudden Expansion," Journal of Fluids Engineering, Transactions, ASME, Vol. 101, 1979.

Tennekes, H., and J. L. Lumley, A First Course in Turbulence, MIT Press, Cambridge, Massachusetts, 1972.

Townsend, A. A., The Structure of Turbulent Shear Flow, Cambridge University Press, London, 1956.

van Bendegom, L., "Some Considerations on River Morphology and River Improvement," De Ingenieur, Vol. 59, B 1-11, 1947.

White, F. M., Viscous Fluid Flow, McGraw-Hill Book Co., Inc., New York, 1974.

NOMENCLATURE

Alphabetic Symbols

c = nondimensional bottom friction coefficients

C = Courant number

C_1 = constant equation (3-24)

C_2 = constant equation (3-24)

C_v = constant equation (3-16)

D = nondimensional dispersion coefficient

$f_{\xi,\eta}$ = quadratic interpolation function

Ft = vector of quantities operated on by the partial derivative with respect to time

Fx = vector of quantities operated on by the partial derivative with respect to the longitudinal coordinate direction, x

Fy = vector of quantities operated on by the partial derivative with respect to the transverse coordinate direction, y

g_i = acceleration due to gravity (0, 0, - g)

G = vector of source quantities

h = water depth

k = turbulence kinetic energy per unit mass

ℓ = turbulent macroscale

P = pressure

P' = turbulent pressure fluctuation

P_h = lateral production term

P_k = vertical production of turbulence energy

P_ε = vertical production of dissipation

q = magnitude of the resultant velocity vector (U,V)

S_x = channel slope in x-direction $(-\partial z_b/\partial x)$

t = time

T_{mn} = depth-integrated effective stress tensor per unit mass (T_{xx}, T_{xy}, T_{yy})

U_* = shear velocity

v_i = time average velocity components (u, v, w)

v_i' = turbulent velocity fluctuations (u', v', w')

V_m = depth-integrated velocity vector (U,V)

W_o = channel half width

W_1 = step height

x_i = coordinate directions (x,y,z)

x_r = reattachment length

X_m = coordinate direction (x,y)

z_b = elevation of the channel bottom above an arbitrary datum

z_o = roughness height

$\tilde{z}$ = location of the depth mean velocity above the channel bottom

Greek Symbols

β = exponent equation (3-11)

δ_{ij} = Kronecker delta

Δ = denotes finite increment

ε = rate of dissipation of turbulence energy per unit mass

ε' = fluctuations of the rate of dissipation per unit mass

η = nondimension local coordinate, $y/\Delta s$

θ = angle that lies between the direction resultant velocity vector, q and the x-axis

κ = von Karman's universal constant

ν = kinematic viscosity of water

ν_t = effective turbulent eddy viscosity

ξ = nondimensional local coordinate, $x/\Delta s$

ρ = mass density of water

σ_k = constant equation (3-19)

σ_ε = constant equation (3-24)

σ_{ij} = shear stress tensor per unit mass

Σ_{mn} = depth-integrated turbulent stress tensor

τ_{bm} = bottom stress vector

ϕ = arbitrary scalar function

Subscripts

a = denotes evaluation of functions at the water surface

b = denotes evaluation of functions at the channel bottom

B = bottom of finite control cell

i = tensor notation index

j = tensor notation index

L = left face of finite control cell

m = tensor notation index

n = tensor notation index

r = tensor notation index

R = right face of finite control cell

s = tensor notation index

T = top of finite control cell

w = near wall value

Superscripts

n = time level

′ = turbulent fluctuation

^ = depth mean value

~ = depth varing two-dimensional quantity

* = cell face variation

Operations

$\overline{}$ = time average

$\underline{}$ = spatial average over control cell

$( )_R$ = right cell face average

$( )_L$ = left cell face average

$( )_T$ = top cell face average

$( )_B$ = bottom cell face average

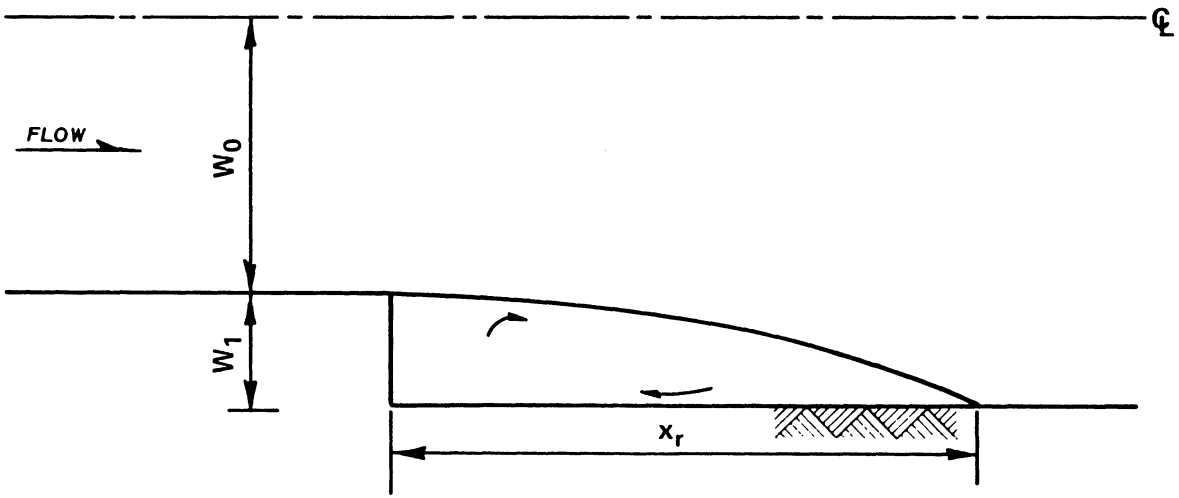

Figure 1. Two-dimensional definition sketch for a channel expansion.

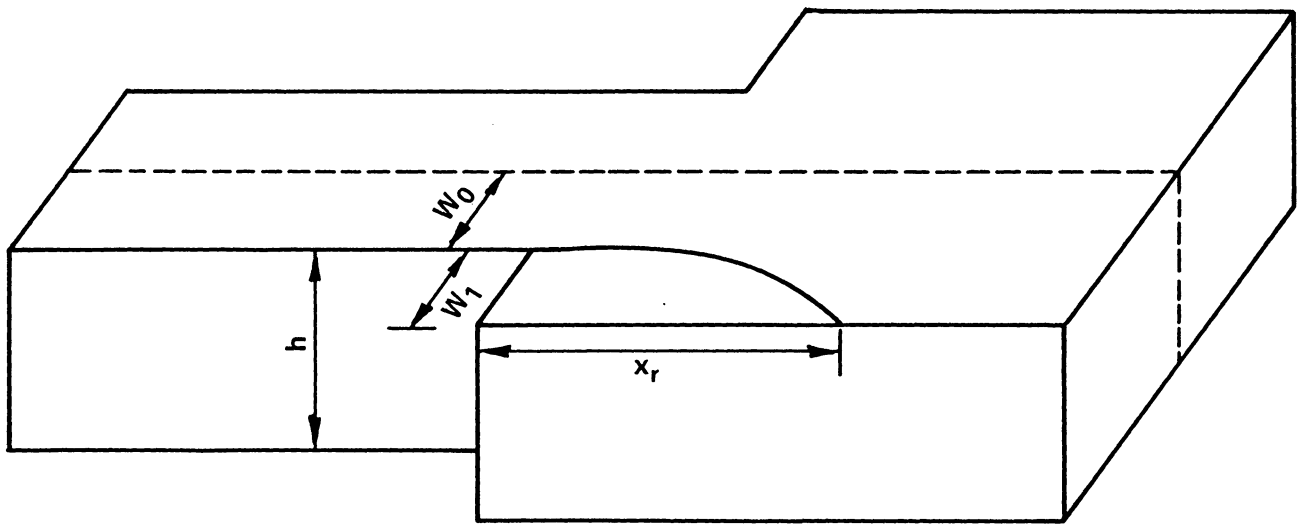

Figure 2. Three-dimensional definition sketch for a channel expansion.

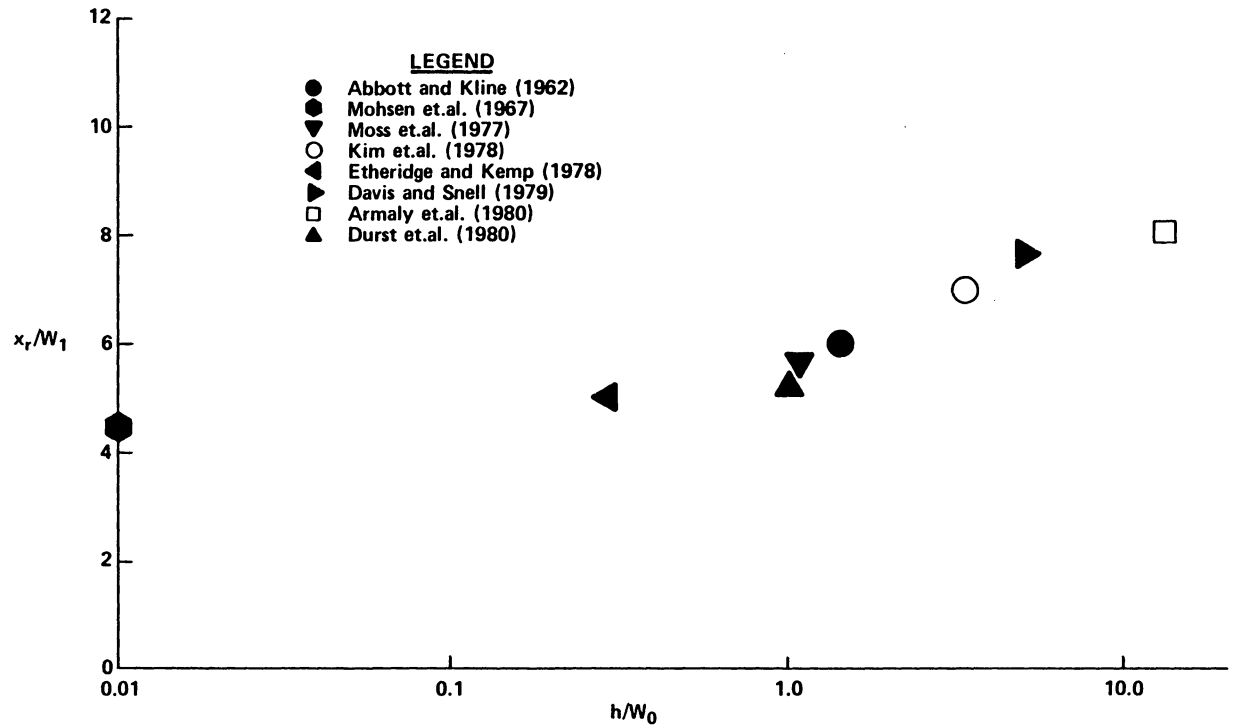

Figure 3. Experimental measurements of nondimensional reattachment lengths versus the inlet channel aspect ratio.

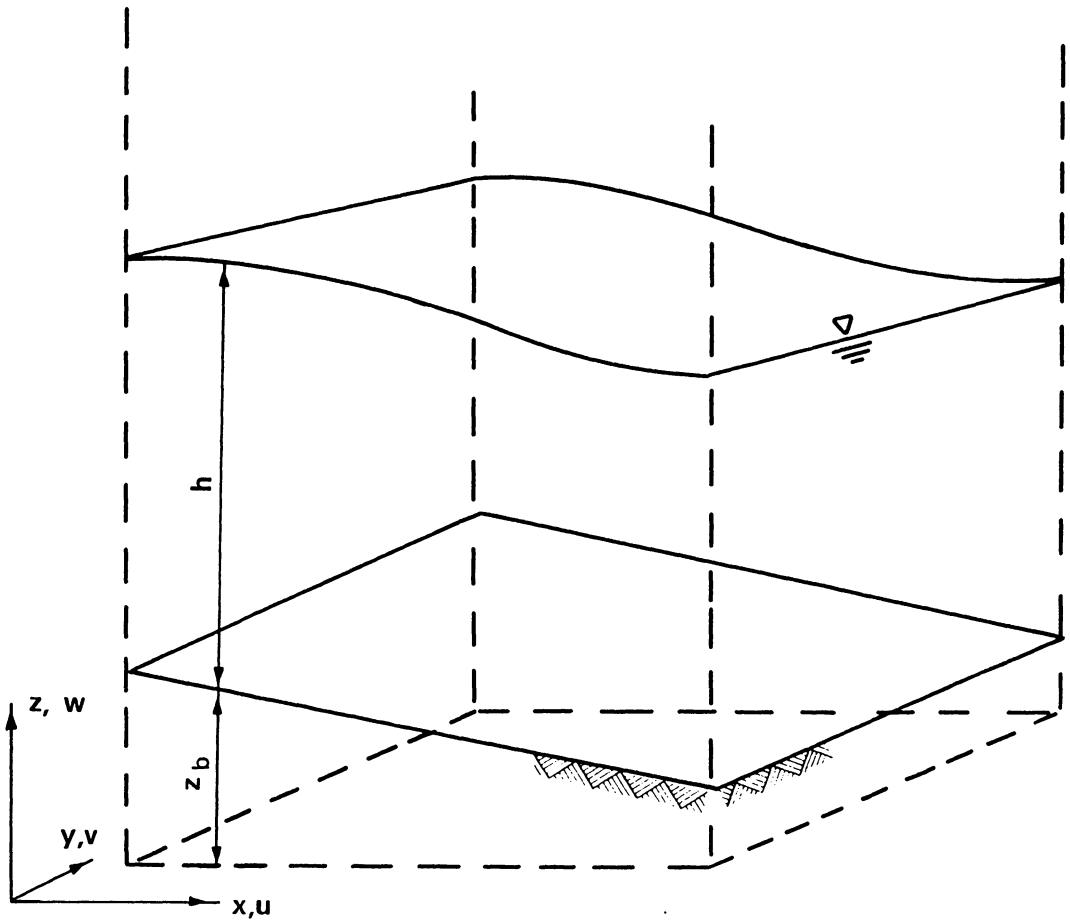

Figure 4. Definition sketch for a Cartesian coordinate system with a free surface.

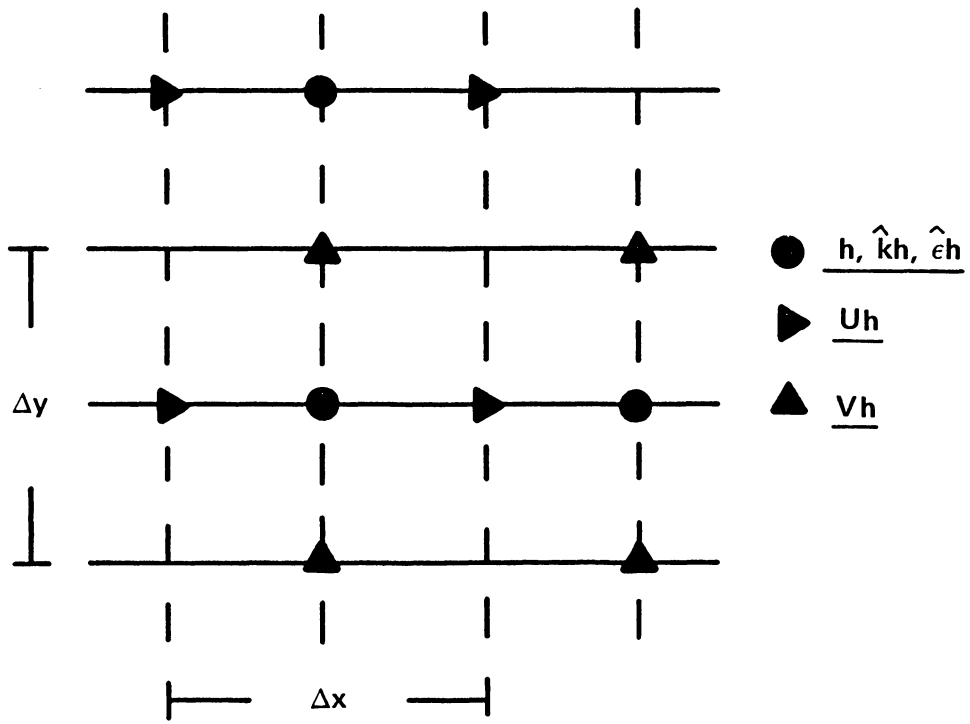

Figure 5. Computational grid.

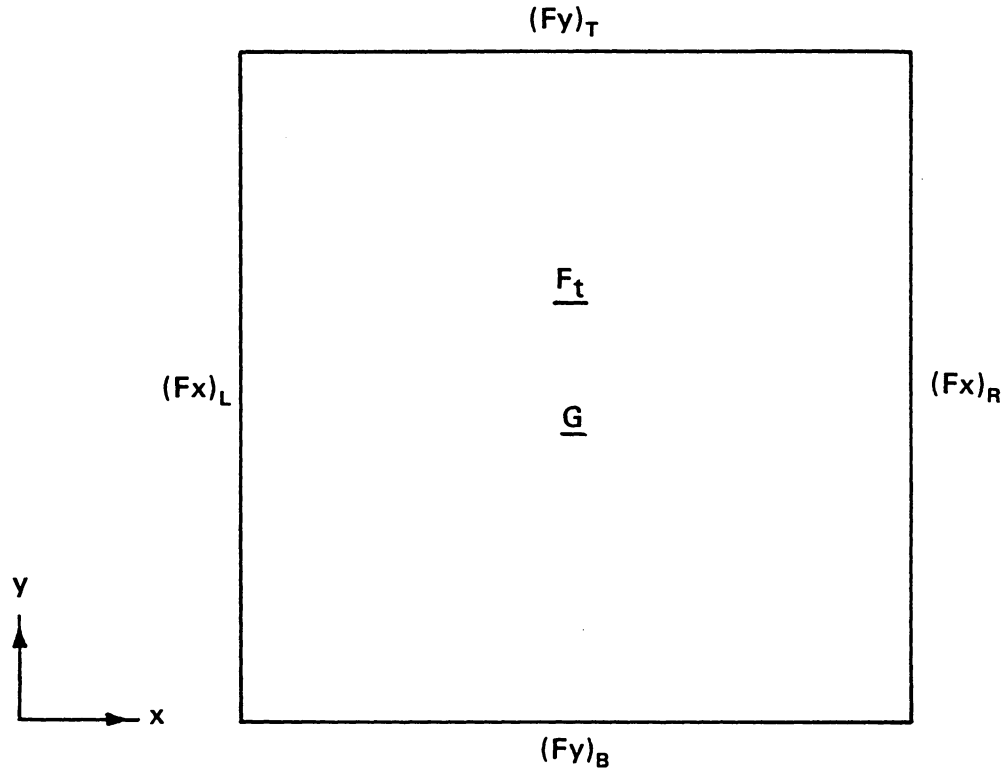

Figure 6. Distribution of cell and cell face average quantities.

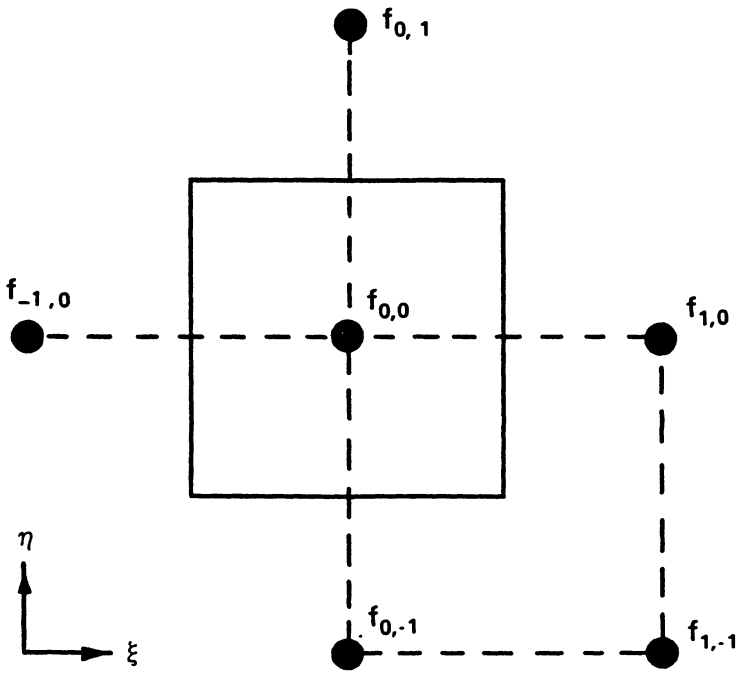

Figure 7. Nodel information required to compute example right cell face average.

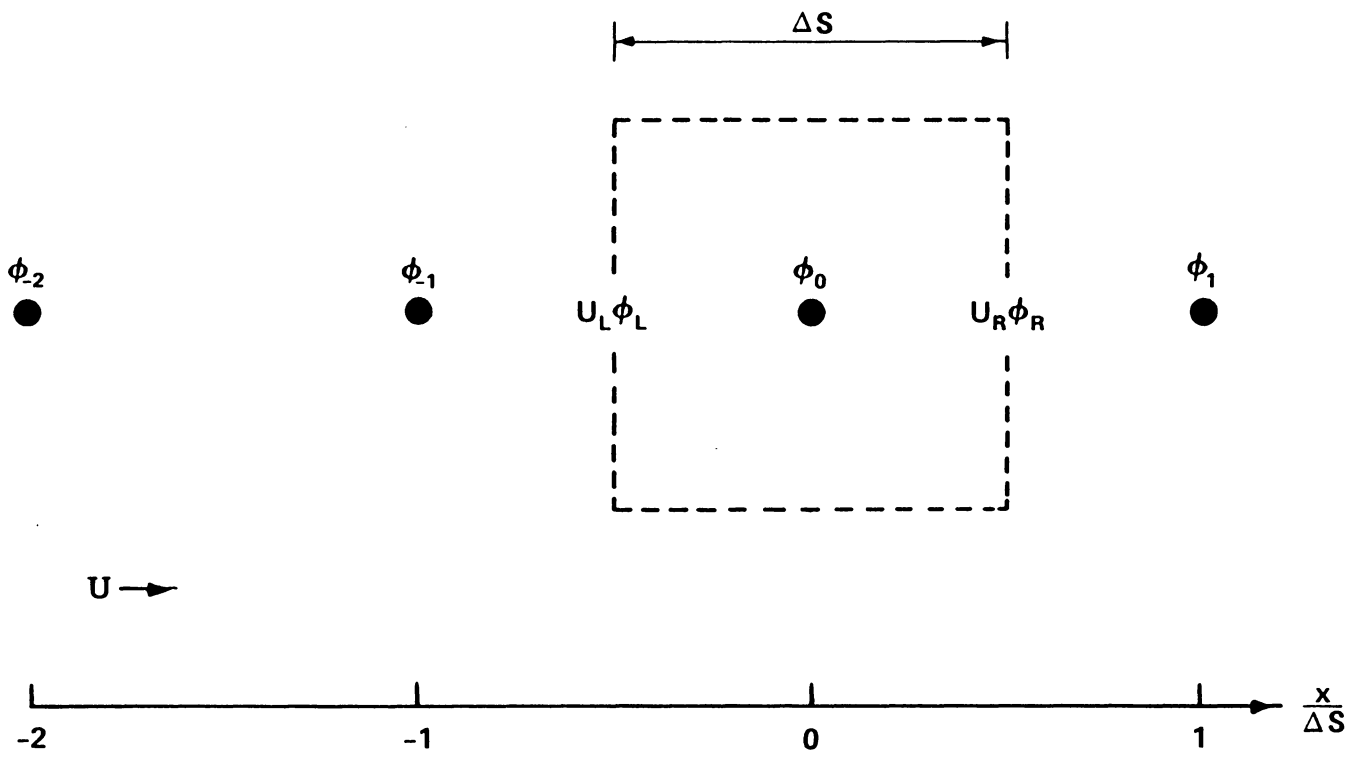

Figure 8. Definition sketch for the convective stability analysis.

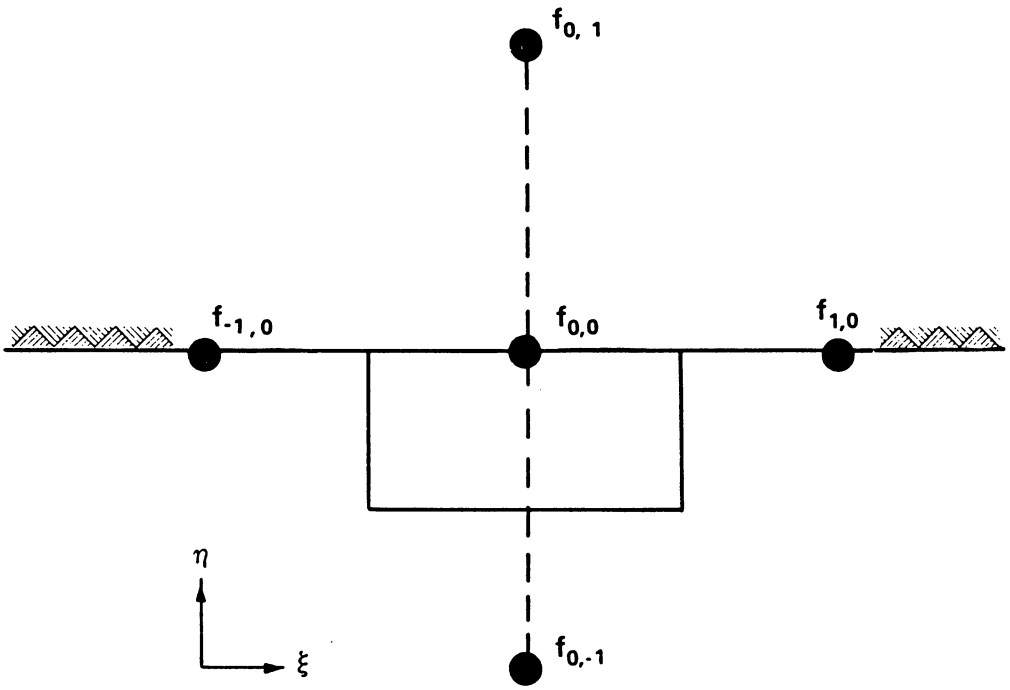

Figure 9. Distribution of the normal velocity component grid points about a wall boundary.

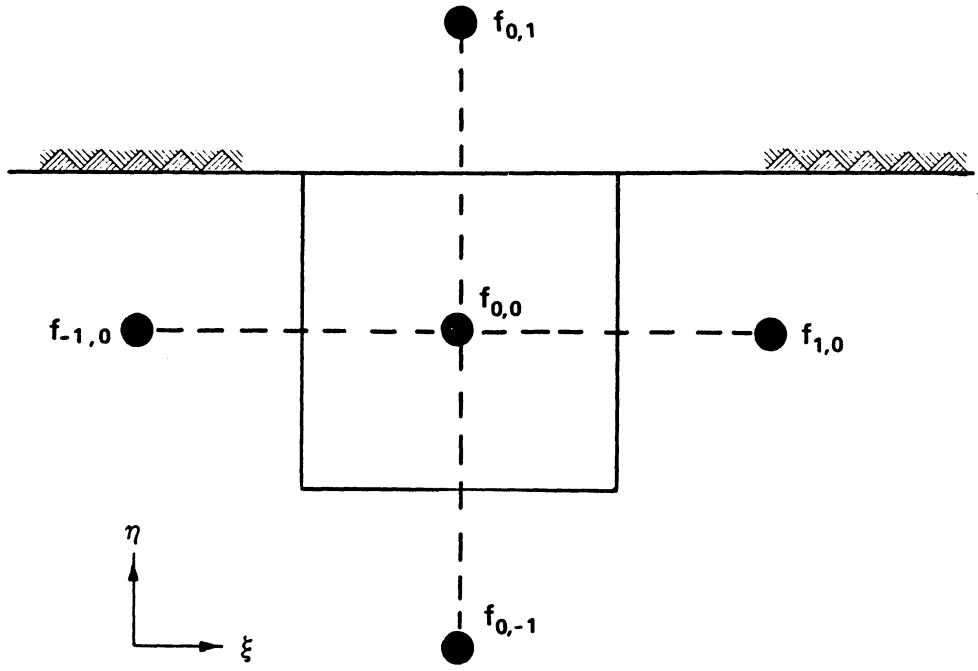

Figure 10. Distribution of the streamwise velocity component and water surface elevation grid points about a wall boundary.

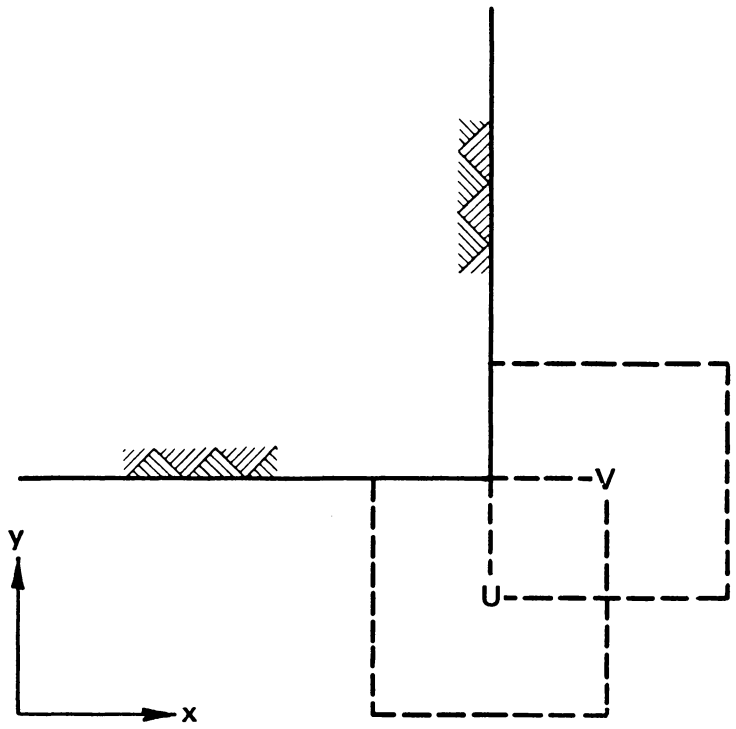

Figure 11. Computational cells that require modification of the "wall function" boundary specification.

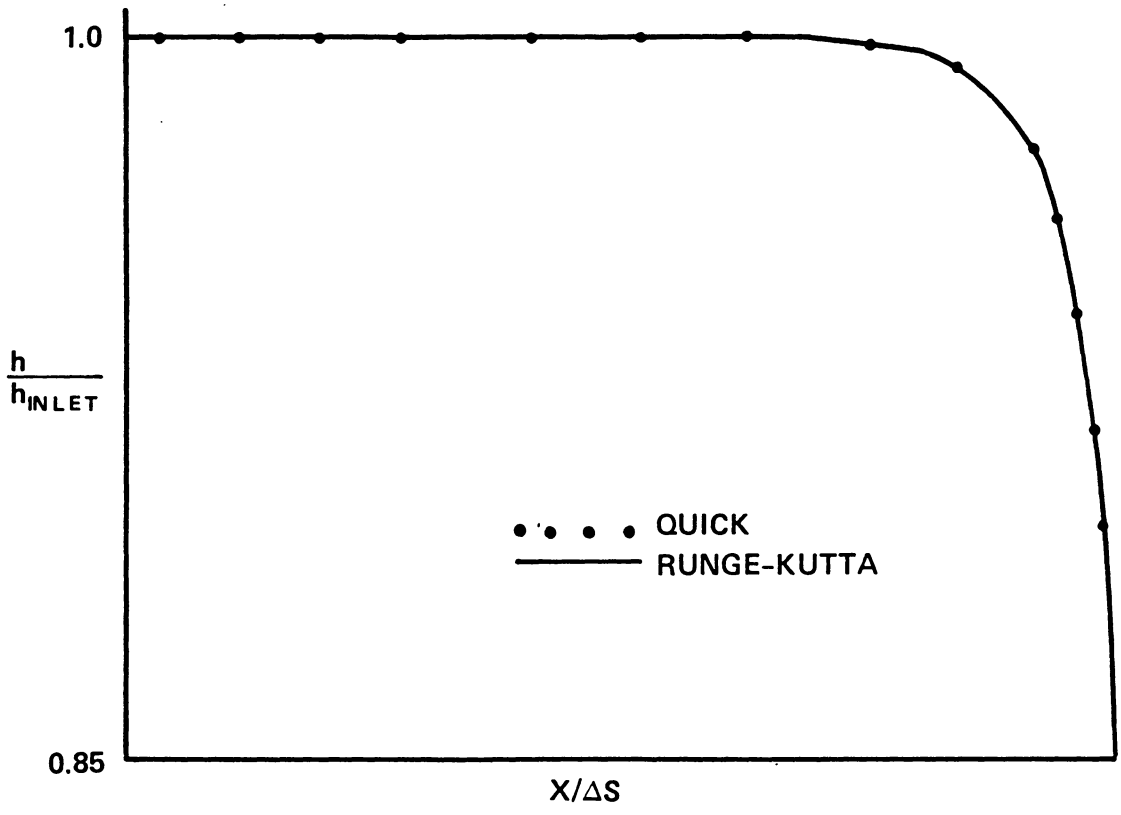

Figure 12. Comparison of water surface profile simulations.

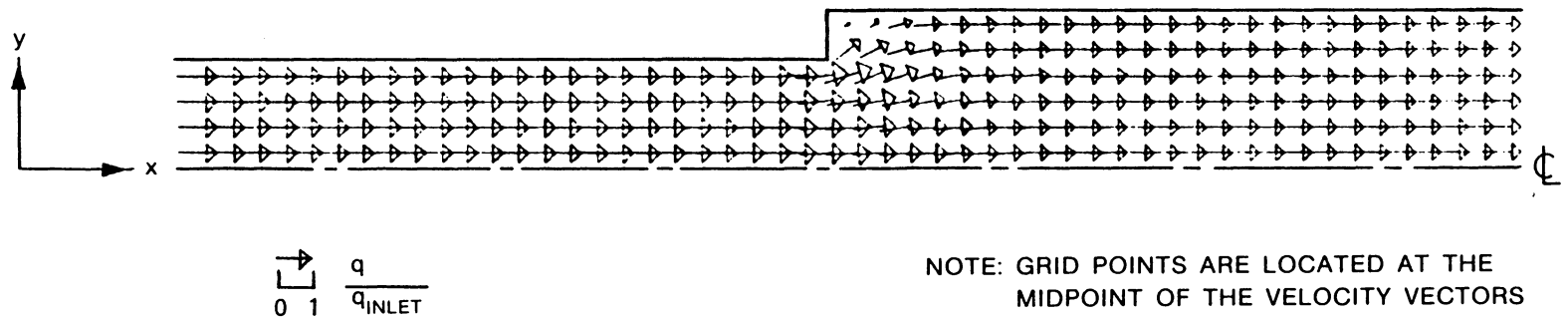

Figure 13. Depth-averaged velocity field for the channel expansion simulation with effective stresses neglected.

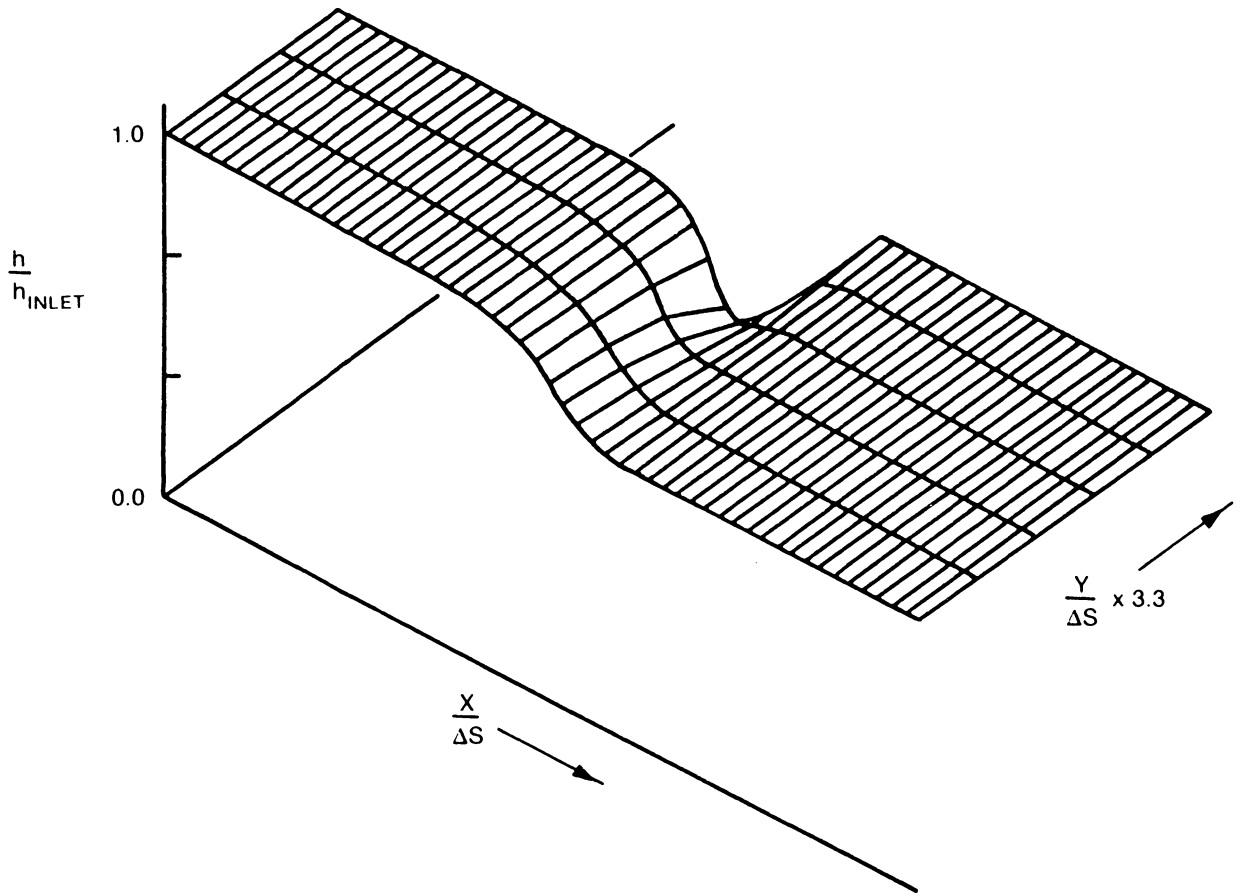

Figure 14. Water surface elevations for the channel expansion simulation with effective stresses neglected.

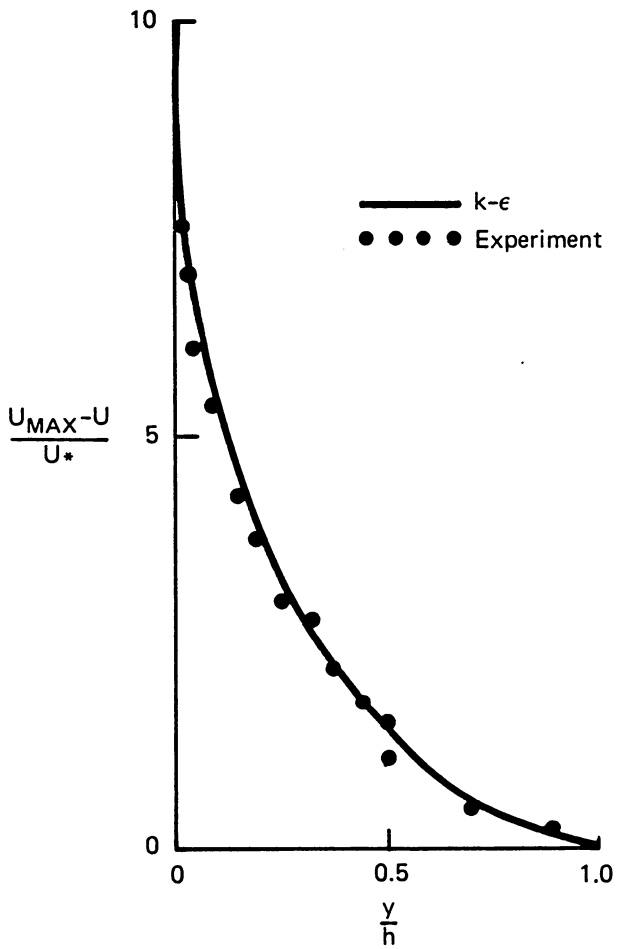

Figure 15. Comparison of model predictions with the experimental velocity defect measurements of Nakagawa et al. (1975).

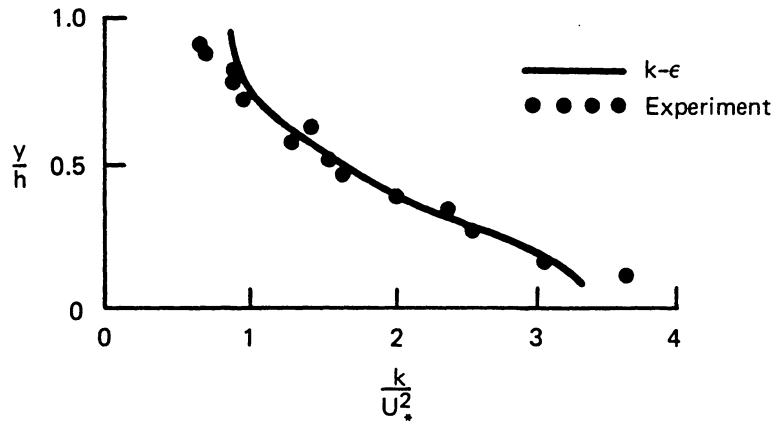

Figure 16. Comparison of model predictions with the experimental turbulence kinetic energy measurements of Nakagawa et al. (1975).

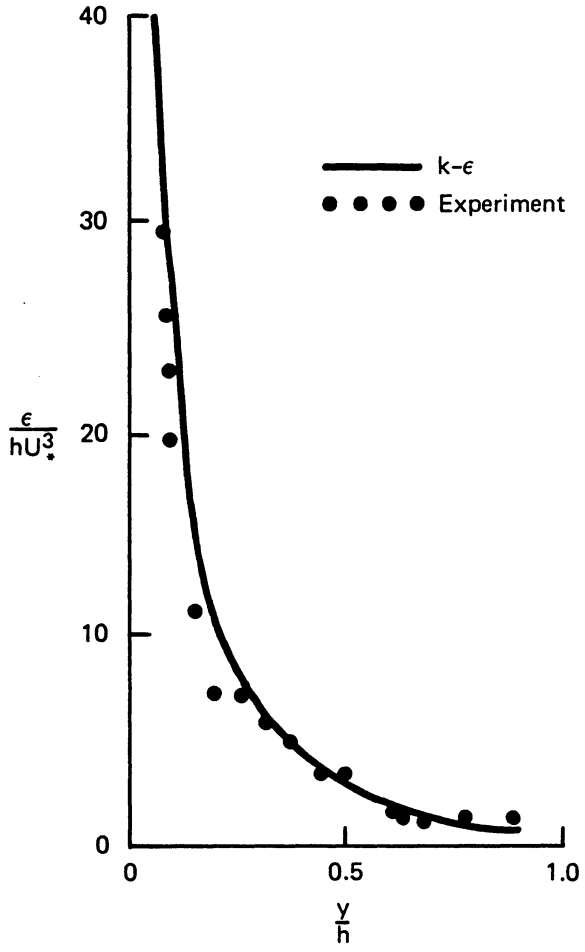

Figure 17. Comparison of model predictions with the experimental energy dissipation rate measurements of Nakagawa et al (1975).

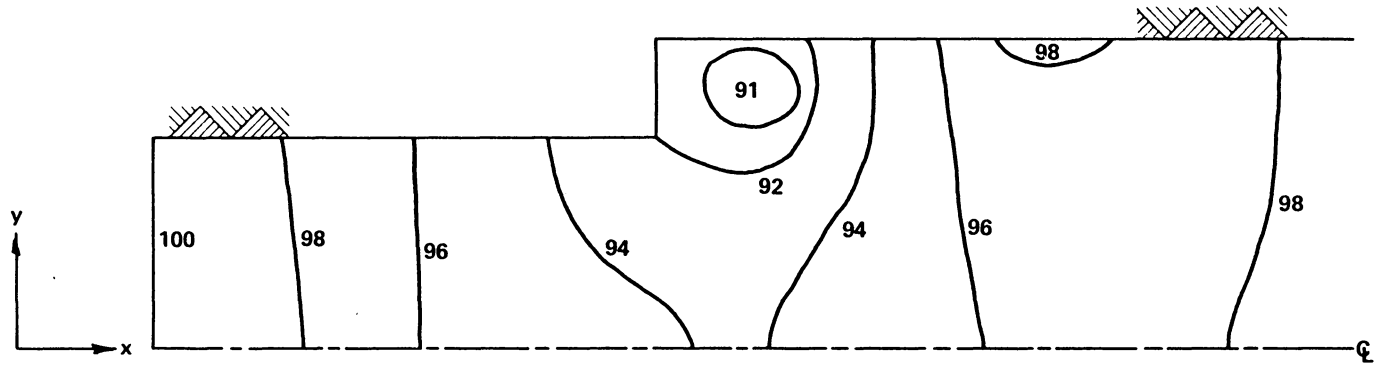

Figure 18. Water surface elevations in percent of the upstream boundary depth for the standard ($k - \epsilon$) turbulence closure simulation.

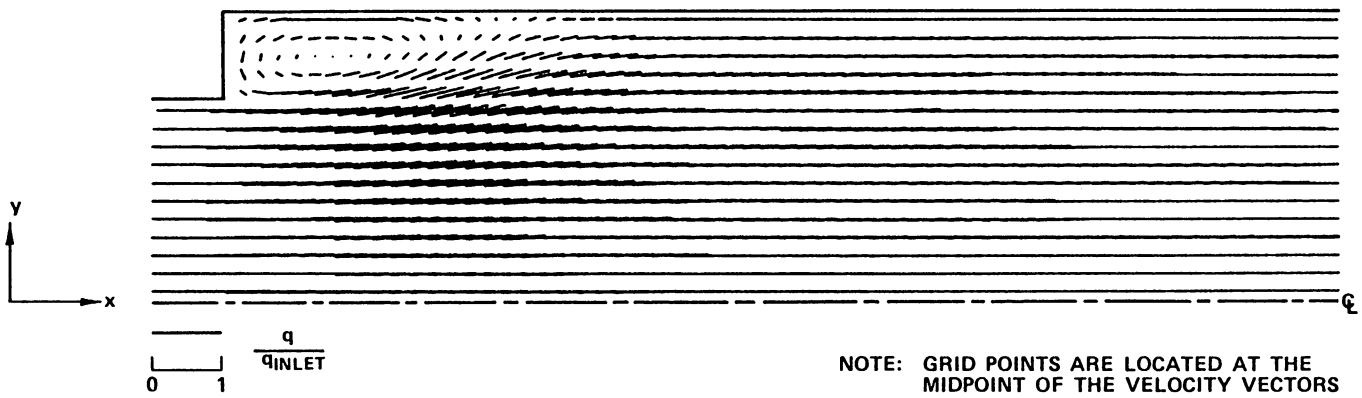

Figure 19. Depth-averaged velocity field for the standard ($k - \epsilon$) turbulence closure simulation.

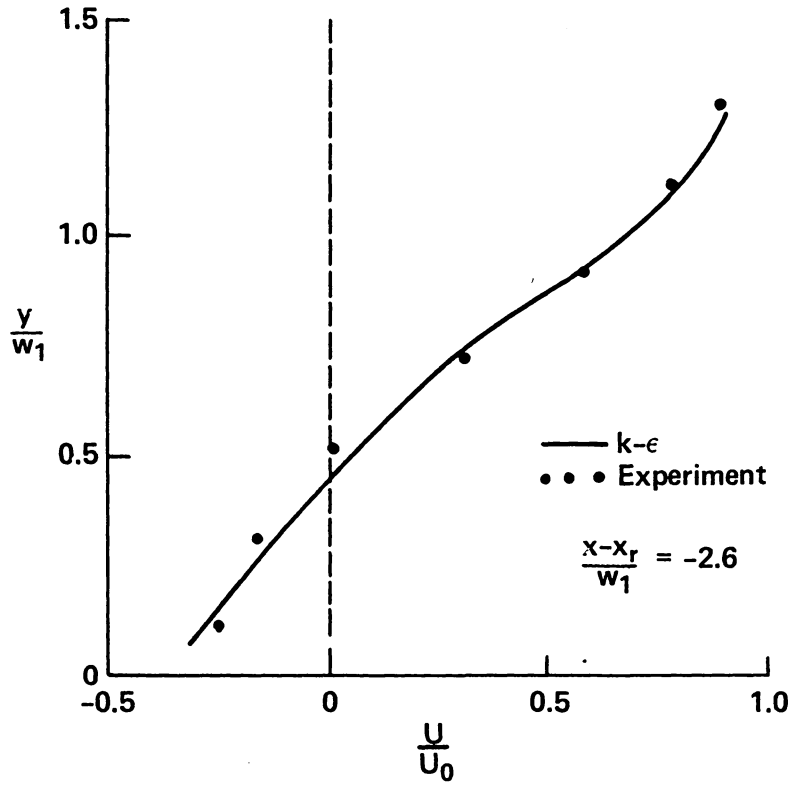

Figure 20. Comparison of standard (k - ϵ) model predictions with the experimental velocity measurements of Moss et al. (1977).

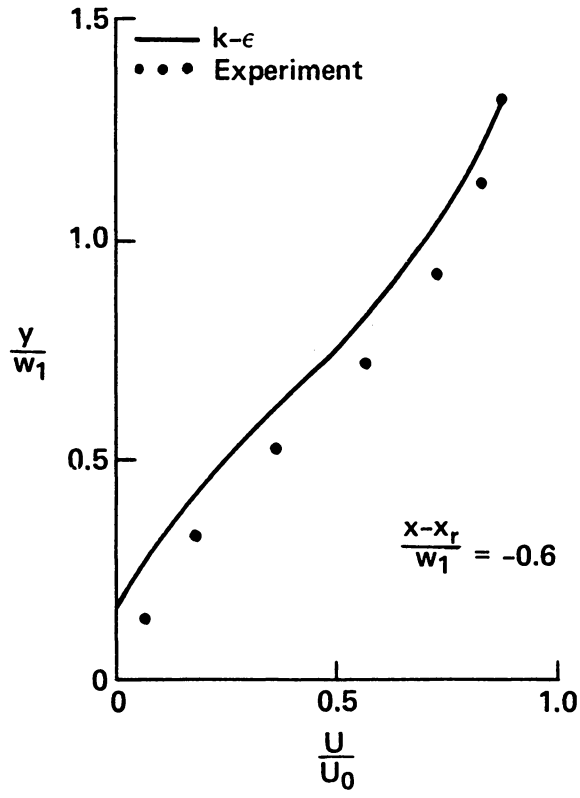

Figure 21. Comparison of standard (k - ϵ) model predictions with the experimental velocity measurements of Moss et al. (1977).

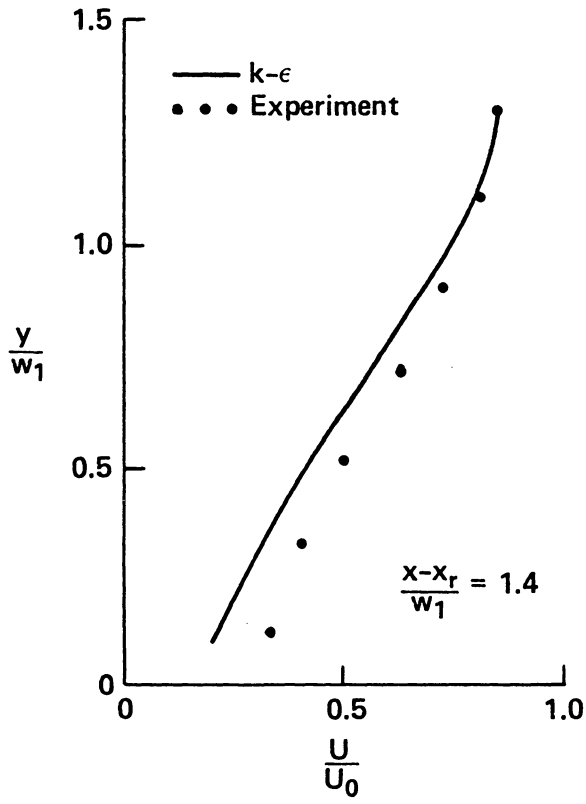

Figure 22. Comparison of standard (k - ϵ) model predictions with the experimental velocity measurements of Moss et al. (1977).

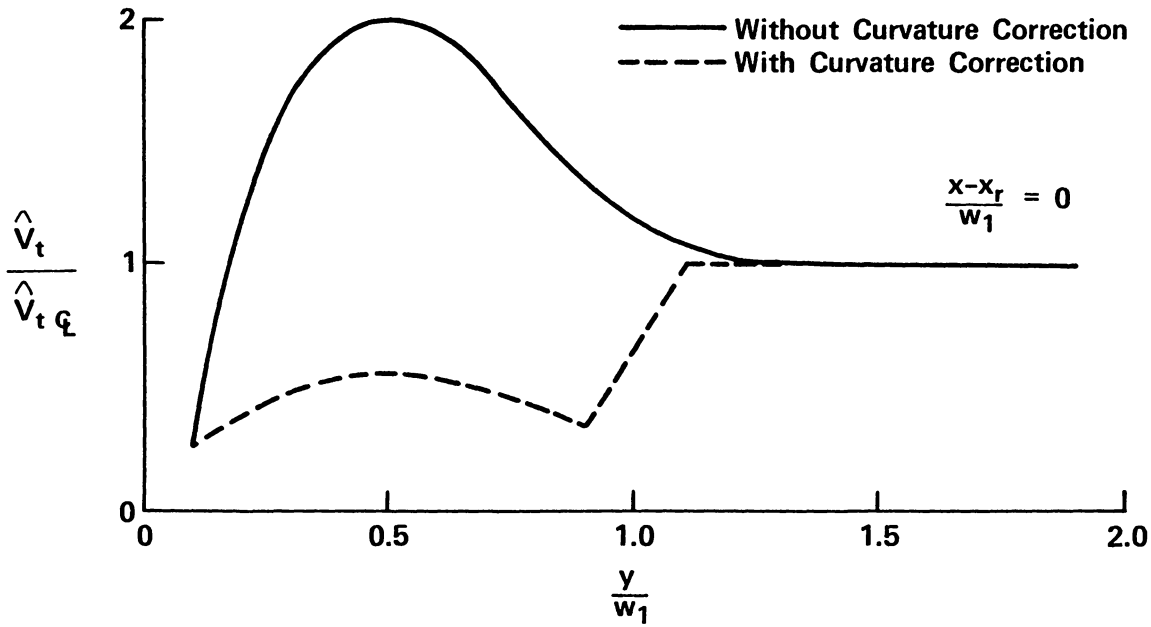

Figure 23. Comparison of predicted eddy viscosities with and without curvature correction at the reattachment point.

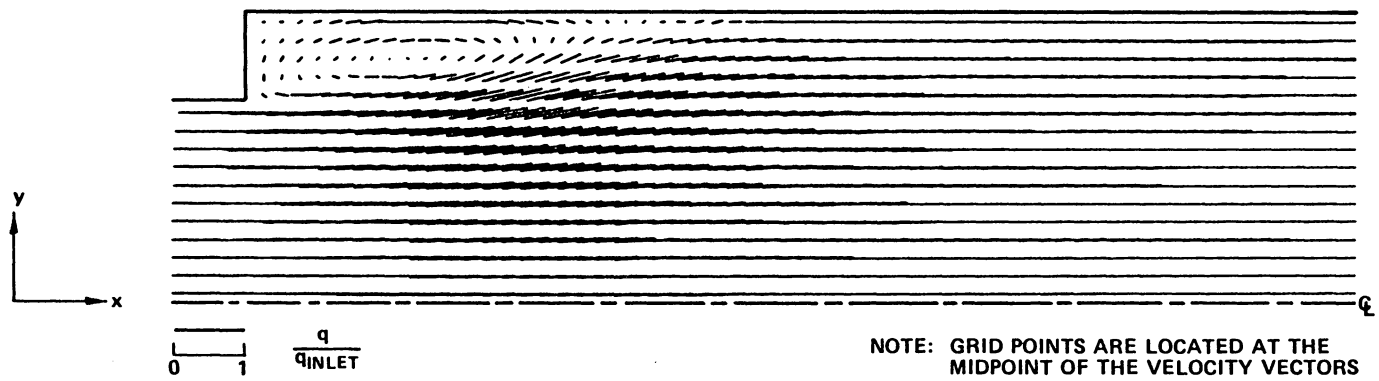

Figure 24. Depth-averaged velocity field for curvature corrected (k - ϵ) turbulence closure simulation.

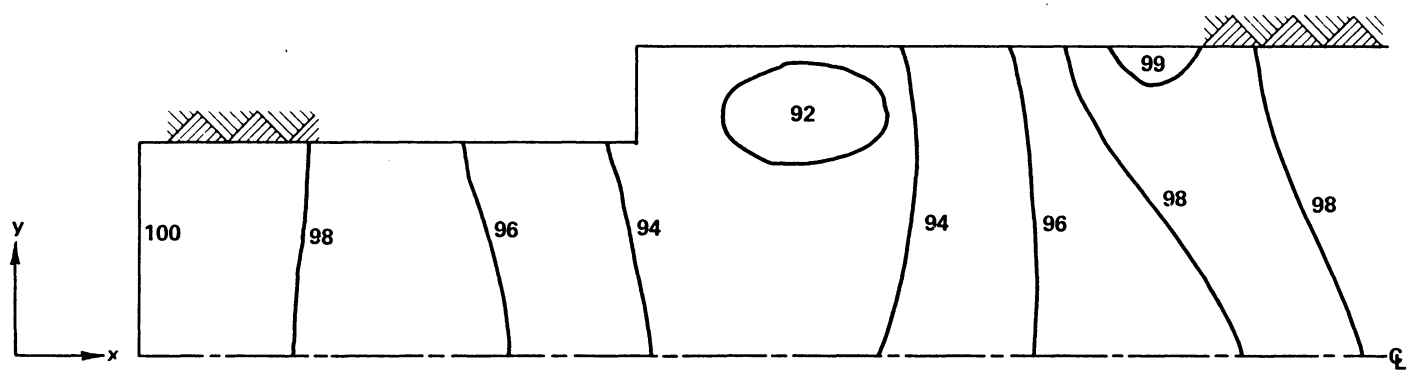

Figure 25. Water surface elevations in percent of the upstream boundary depth for the curvature corrected ($k - \epsilon$) turbulence closure simulation.

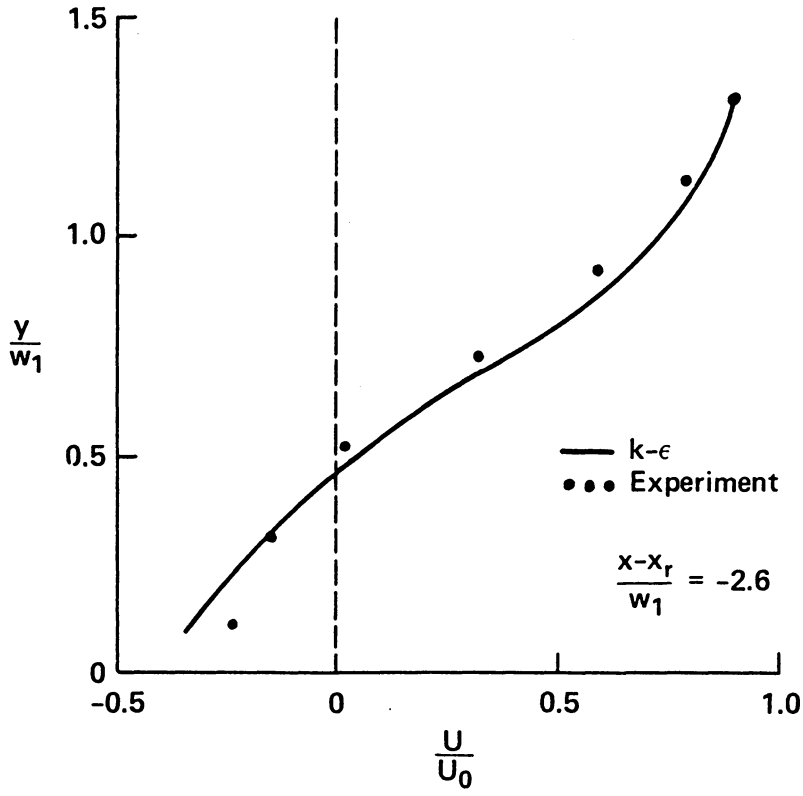

Figure 26. Comparison of curvature corrected (k - ϵ) model predictions with the experimental velocity measurements of Moss et al. (1977).

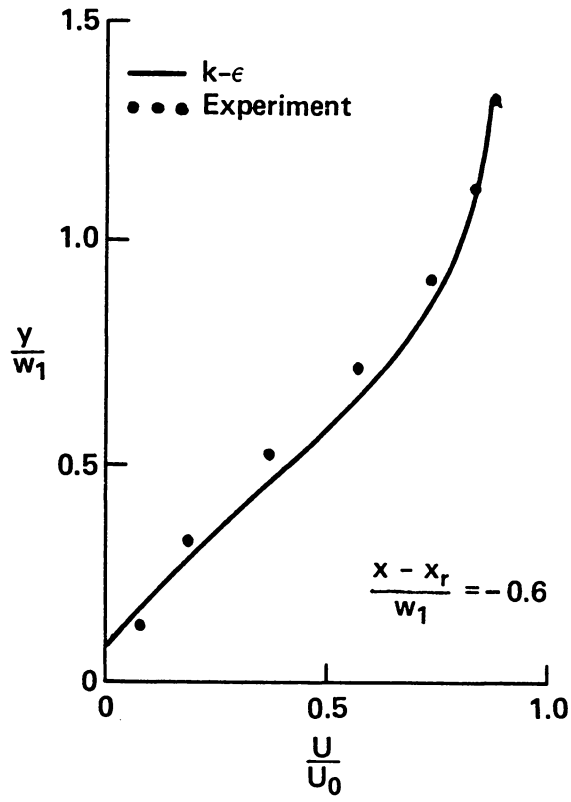

Figure 27. Comparison of curvature corrected (k - ϵ) model predictions with the experimental velocity measurements of Moss et al. (1977).

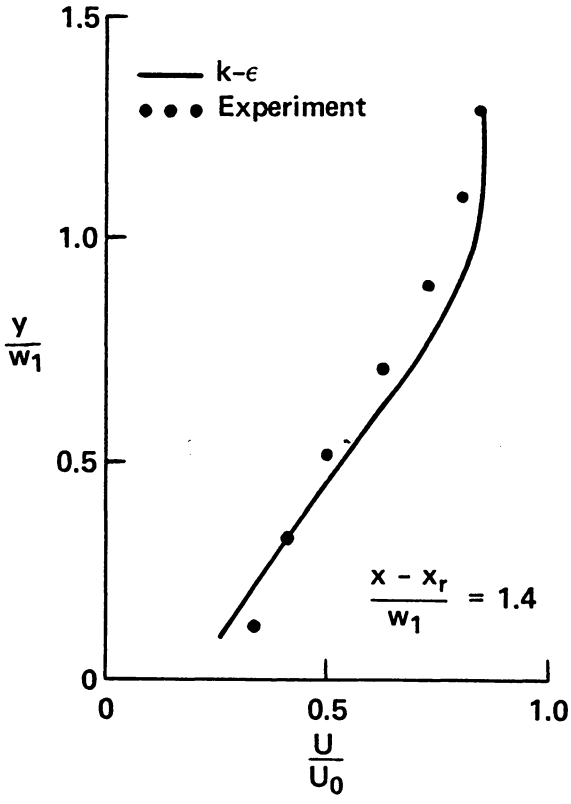

Figure 28. Comparison of curvature corrected (k - ϵ) model predictions with the experimental velocity measurements of Moss et al. (1977).

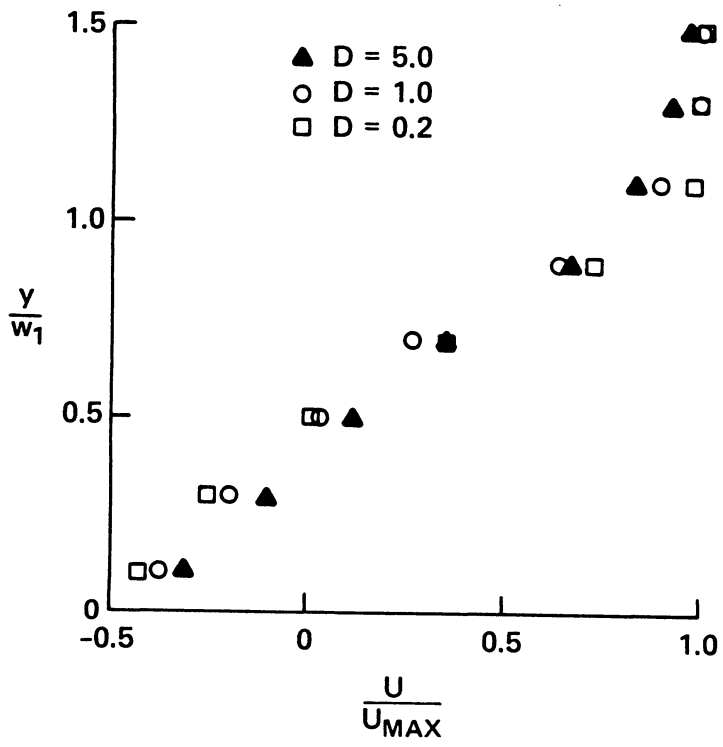

Figure 29. Comparison of predicted velocity profiles within the recirculation region for varying nondimensional dispersion coefficient.

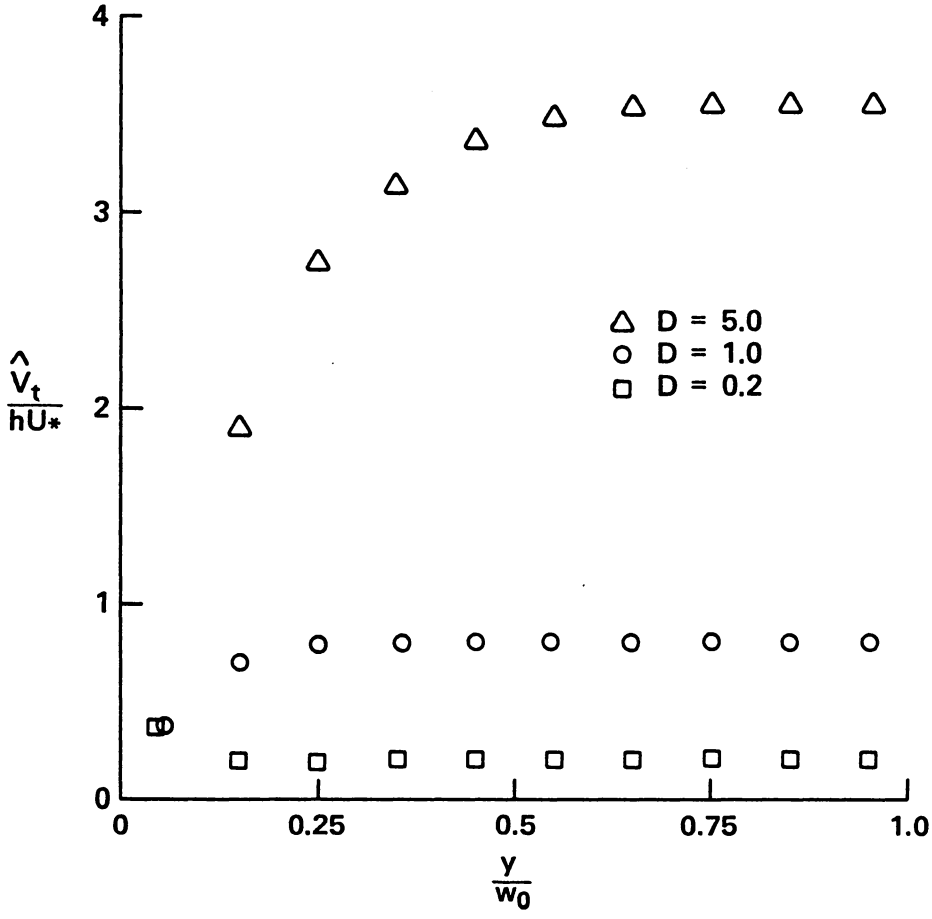

Figure 30. Comparison of predicted eddy viscosities at the upstream boundary for varying nondimensional dispersion coefficient.

The vita has been removed from the scanned document

A NUMERICAL SIMULATION OF TWO-DIMENSIONAL SEPARATED FLOW IN A SYMMETRIC OPEN-CHANNEL EXPANSION USING THE DEPTH-INTEGRATED TWO-EQUATION (k-ε) TURBULENCE CLOSURE MODEL

by

Raymond Scott Chapman

(ABSTRACT)

Many of the free surface flow problems encountered by hydraulic engineers can be suitably analyzed by means of the depth-integrated equations of motion. A consequence of adopting a depth-integrated modeling approach is that closure approximations must be implemented to represent the so-called effective stresses.

The effective stresses consist of the depth-integrated viscous stresses, which are usually small and neglected, the depth-integrated turbulent Reynold's stresses, and additional stresses resulting from the depth-integration of the nonlinear convective accelerations (here after called momentum dispersion). Existing closure schemes for momentum dispersion lack sufficient numerical and experimental verification to warrant consideration at this time, so consequently, attention is focused on examining closure for the depth-integrated turbulent Reynold's stresses.

In the present study, an application at the depth-integrated (k-ε) turbulence model is presented for separated flow in a wide, shallow, rectangular channel with an abrupt expansion in width. The well-known numerical problems associated with the use of upwind and central finite differences for convection is overcome by the adoption of the spatially third-order accurate QUICK finite difference technique. Results presented show that modification of the depth-integrated (k-ε) turbulence closure model for streamline curvature leads to significant improvement in the agreement between model predictions and experimental measurements.